Tectonic-hydrothermal brecciation associated with calcite precipitation and permeability destruction in Mississippian carbonate reservoirs, Montana and Wyoming

David A. Katz, Gregor P. Eberli, Peter K. Swart, and Langhorne B. Smith Jr.

ABSTRACT

The Mississippian Madison Formation contains abundant fracture zones and breccias that are hydrothermal in origin based on their morphology, distribution, and geochemical signature. The hydrothermal activity is related to crustal shortening during the Laramide orogeny. Brecciation is accompanied by dedolomitization, late-stage calcite precipitation, and porosity occlusion, especially in outcrop dolomites. The tectonic-hydrothermal late-stage calcite reduces permeability in outcrops and, potentially, high-quality subsurface reservoir rocks of the subsurface Madison Formation, Bighorn Basin. The reduction of permeability and porosity is increased along the margins of the Bighorn Basin but not predictable at outcrop scale. The destruction of porosity and permeability by hydrothermal activity in the Madison Formation is unique in comparison to studies that document enhanced porosity and permeability and invoke hydrothermal dolomitization models.

Hydrothermal breccias from the Owl Creek thrust sheet are classified into four categories based on fracture density, calcite volume, and clast orientation. Shattered breccias dominate the leading edge of the tip of the Owl Creek thrust sheet in the eastern Owl Creek Mountains, where tectonic deformation is greatest, whereas fracture, mosaic, and chaotic breccias occur throughout the Bighorn Basin. The breccias are healed by calcite cements with $\delta^{18}O$ values ranging between −26.5 and −15.1‰ Peedee belemnite (PDB),

Manuscript received April 18, 2005; provisional acceptance September 15, 2005; revised manuscript received March 6, 2006; final acceptance March 20, 2006.
DOI:10.1306/03200605072

AUTHORS

DAVID A. KATZ ~ *Comparative Sedimentology Laboratory, University of Miami, 4600 Rickenbacker Causeway, Miami, Florida 33149-1098; dkatz@rsmas.miami.edu*

David A. Katz received his B.S. degree from Hamilton College (1999) and his M.S. degree from the Colorado School of Mines (2002) and is currently a Ph.D. candidate at the University of Miami, where he conducts research at the Comparative Sedimentology Laboratory. His research investigates the earliest diagenesis and geochemistry of modern carbonates, dolomitization, and integration of geochemistry with sequence stratigraphy in ancient carbonates.

GREGOR P. EBERLI ~ *Comparative Sedimentology Laboratory, University of Miami, 4600 Rickenbacker Causeway, Miami, Florida 33149-1098; geberli@rsmas.miami.edu*

Gregor P. Eberli is a professor and chair of the Division of Marine Geology and Geophysics at the University of Miami and is the director of the Comparative Sedimentology Laboratory. He received his Ph.D. from the Swiss Institute of Technology (Eidgenössische Technische Hochschule) in Zurich, Switzerland. His field research focuses on sedimentology and sequence stratigraphy of carbonates. In the laboratory, he explores the influence of pore structure on petrophysical properties of carbonates. He was Distinguished Lecturer for AAPG (1996–1997), the Joint Oceanographic Institutions/U.S. Science Advisory Committee (1997–1998), and the European Association of Geoscientists and Engineers (2005).

PETER K. SWART ~ *Comparative Sedimentology Laboratory, University of Miami, 4600 Rickenbacker Causeway, Miami, Florida, 33149-1098; pswart@rsmas.miami.edu*

Peter received his Ph.D. from the University of London in 1980 for work on modern coral reefs. After 3 years at the University of Cambridge, he started a project on dolomite geochemistry at the University of Miami, where he is now a professor of marine geology and geophysics in the Rosenstiel School of Marine and Atmospheric Sciences. His professional interests include carbonate geochemistry and diagenesis, hydrology, and paleoclimatology. He is also a coleader of the Comparative Sedimentology Laboratory.

LANGHORNE B. SMITH JR. ~ *New York State Museum, Room 3124 CEC, Albany, New York 12230; lsmith@mail.nysed.gov*

Langhorne "Taury" Smith heads the Reservoir Characterization Group at the New York State Museum. He holds a B.S. degree from Temple University and a Ph.D. from Virginia Polytechnic Institute and State University and did postdoctoral work at the University of Miami. He also worked for Chevron as a development geologist, and his current research interests are focused on carbonate reservoir characterization and hydrothermal alteration of carbonate reservoirs.

ACKNOWLEDGEMENTS

We first thank Brian Coffey and an anonymous reviewer for their constructive reviews of this document. We also thank the industrial associates of our Comparative Sedimentology Laboratory Consortium for financial support of this project. In addition, we especially appreciate Chevron's generous support of the color reproduction costs for this manuscript. The first author also thanks the coauthors, Eugene Rankey, Mark Sonnenfeld, and Matthew Buoniconti for thoughtful reviews and discussion.

indicating that the cements were derived from isotopically depleted fluids with elevated temperatures. In the chaotic and mosaic breccia types, large rotated and angular clasts of the host rock float in the matrix of coarse and nonzoned late-stage calcite. This appearance, combined with similar $\delta^{18}O$ values across even large calcite veins, indicates that the calcite precipitated rapidly after brecciation. Values for $\delta^{13}C$ (~5–12 ‰ PDB) from the frontal part of the Owl Creek thrust sheet indicate equilibrium between methane and CO_2-bearing fluids at about 180°C. Fluid inclusions from the eastern basin margin show that these cements are in equilibrium with fluids having minimum temperatures between 120 and 140°C and formed from relatively low-salinity fluids, less than 5 wt.% NaCl. Strontium isotope ratios of these hydrothermal fluids are more radiogenic than proposed values for Mississippian seawater, suggesting that the fluids mixed with felsic-rich basement before migrating vertically into the Madison Formation.

We envisage that the tectonic-hydrothermal late-stage calcite-cemented breccias and fractures originated from undersaturated meteoric groundwaters that migrated into the burial environment while dissolving and incorporating Ca^{2+} and CO_3^{2-} and radiogenic Sr from the dissolution of the surrounding carbonates and the felsic basement, respectively. In the burial environment, these fluids were heated and mixed with hypersaline brines from deeply buried parts of the basement. Expulsion of these fluids along basement-rooted thrust faults into the overlying strata, including the Madison Formation, occurred most likely during shortening episodes of the Laramide orogeny by earthquake-induced rupturing of the host rock. The fluids were injected forcefully and in an explosive manner into the Madison Formation, causing brecciation and fracturing of the host rock, whereas the subsequent and sudden decrease in the partial pressure of CO_2 caused the rapid precipitation of calcite cements.

The explosive nature of hydrothermal fluid migration ultimately produces heterogeneities in reservoir-quality carbonates. In general, flow units in the Madison Formation are related to sequence boundaries, which create vertical subdivisions in the porous dolomite. The late-stage calcite cement surrounds hydrothermal breccia clasts and invades the dolomite, reducing porosity and permeability of the reservoir-quality rock. As a consequence, horizontal flow barriers and compartments are established that are locally unpredictable in their location and extent and regionally predictable along the margins of the Bighorn Basin.

INTRODUCTION

Understanding the paragenetic sequence of geologic events in and around sedimentary basins can improve our knowledge of geologic hazards that affect the success of hydrocarbon and groundwater aquifer exploration. Orogenic processes in North American Laramide

basins are responsible for introducing diagenetic and hydrological heterogeneities between and within basins (Doremus, 1986; Jarvis, 1986; Spencer, 1986; Huntoon, 1993) and can function as an analog to other sedimentary basins, which developed in compressional regimes where crustal thickening or thrust stacking can lead to progressive dewatering and maintenance of suprahydrostatic pressure gradients in the fluid (Sibson, 1990). Tectonic brecciation and fracturing, followed by hydrothermal cementation of the host rock in these settings, result during episodes of fault slip, and evidence for this diagenesis may have been overlooked in the past (Sibson, 1990). Westphal et al. (2004) suggest that the tectonic-hydrothermal processes significantly impact the lateral connectivity in a fluid or gas reservoir.

The focus of this study is the corridors of locally unpredictable, vertical to subvertical breccias and fractures healed by late-stage calcite. We aim to prove that the breccias are explosive in nature, and that the associated hydrothermal fluids precipitated the calcite. To reach this goal, we will (1) describe the various types of tectonic-hydrothermal brecciation and their regional distribution; (2) constrain the hydrothermal character of the Laramide late-stage calcite by integrating petrography, stable isotope geochemistry, fluid-inclusion analysis, and strontium isotope geochemistry; (3) show how the tectonic-hydrothermal activity is predictable on a regional scale; and (4) document how tectonic-hydrothermal brecciation and late-stage calcite precipitation reduce porosity and permeability, which produces locally unpredictable heterogeneities in otherwise high-quality reservoir dolomites of the Mississippian Madison Formation.

Fluid flow along basement-rooted faults produces a variety of secondary alterations in carbonate rocks. For example, hydrothermal leaching and subsequent dolomitization from saline hydrothermal fluids rising along wrench and strike-slip basement-rooted faults (Karachaganak platform) can enhance porosity and permeability in some hydrocarbon reservoirs (Bliefnick et al., 2000). In contrast, Kislak et al. (2001) showed evidence that upward migration of hydrothermal fluids can be explosive in nature, causing brecciation and fracturing of the host rock and subsequent rapid hydrothermal calcite cementation that heals the breccias. They described such late-stage healed breccias in the Mississippian Madison Formation of Wyoming. Westphal et al. (2004) noted the unpredictable pattern of the hydrothermal breccias that cut through the strata in a manner reminiscent of dikes and explosive intrusions. They also documented how the calcite cementation reduces porosity and permeability that introduces unwelcome uncertainties for reservoir-quality assessment at the field scale.

Previous studies (Elrick, 1990; Sonnenfeld, 1996a, b; Smith et al., 2004; Westphal et al., 2004) of the Mississippian Madison Formation documented its facies and stratigraphic architecture. The Madison Formation consists of shallow-water carbonates deposited on a laterally extensive ramp with rather uniform facies belts up to 100 km (60 mi) wide (Westphal et al., 2004). Several orders of sea level change produced a sequence-stratigraphic architecture of landward-stepping facies belts during transgressive periods and seaward progradation during regressive periods (Sonnenfeld, 1996a). Patterns of early diagenesis and dolomitization largely follow this sequence-stratigraphic pattern (Sonnenfeld 1996a, b; Smith et al., 2004). In addition, the distribution of fabric-selective dolomite is intimately tied to sequence stratigraphy in both subsurface and outcrop of the Madison Formation (Smith et al., 2004), resulting in comparable rock fabrics and porosity evolution (Crockett, 1994; Moore, 1995, 2001). As a result, the Madison Formation contains flow units that are bounded by laterally continuous stratigraphic and diagenetic boundaries, which are locally predictable in outcrop.

METHODS

Primary data are from outcrops along a northwest-southeast transect through the margins of the Bighorn Basin from the eastern Owl Creek Mountains of central Wyoming and near the southern entrance of Yellowstone National Park, northwestern Wyoming (Figure 1). Data for this study are derived from core plugs collected during fieldwork for the Smith et al. (2004) and Westphal et al. (2004) studies and from additional core plugs and hand samples that were collected at Sheep Mountain, Shoshone Canyon, and Wind River Canyon using a handheld and gas-powered coring drill. The sampling strategy was determined by locations of outcropping tectonic fractures and breccias, constrained by a sequence-stratigraphic framework (Figure 2) (Elrick, 1990; Sonnenfeld, 1996a, b; Smith et al., 2004). Late-stage calcite from outcrop was compared with Madison subsurface core housed at the U.S. Geological Survey Corelabs, Denver, Colorado. These locations include the northwestern Bighorn Basin–Elk Basin field (EBM 122 and EBM 8; Sonnenfeld, 1996b), and the only subsurface

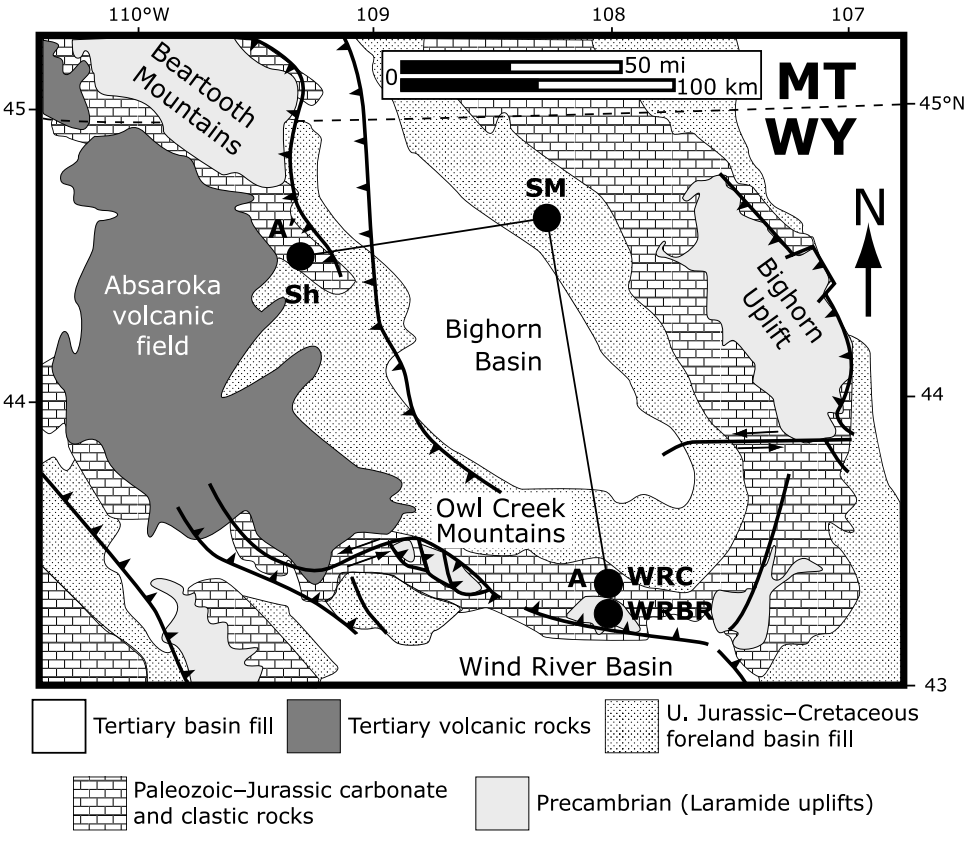

Figure 1. Geologic map of outcrop locations and approximate location of large-magnitude faults (solid black lines with teeth) from Paylor and Yin (1993) and Stone (1993). Teeth point toward the hanging-wall block. AA′ is a cross section of the measured sections displayed in Figure 2. WRC = Wind River Canyon; WRBR = Wind River Boysen reservoir; Sh = Shoshone Canyon; and SM = Sheep Mountain anticline. This map has been modified from Witkind and Grose (1972).

location with any late-stage calcite-cemented breccias and fractures is located in the northern fault-severed margin of the Wind River Basin (Devon Energy, Beaver Creek 137), central Wyoming.

Porosity and Permeability

The porosity and permeability data presented here are from the Smith et al. (2004) and Westphal et al. (2004) studies. Porosity of outcrop and subsurface samples was determined by helium injection or weight-volume relationships. Permeability data are derived from nitrogen flow measurements.

Stable Carbon and Oxygen Isotopes

Late-stage calcites, modern speleothem deposits from Montana, and three varieties of what we interpreted as Mississippian meteoric calcite, as well as Mississippian marine calcite, were sampled using a 25-μm-wide microdrill. Medium-crystalline (75–200-μm-wide) non-fabric-selective and partially fabric-destructive dolomite and finely crystalline (5–75-μm-wide), fabric-selective dolomite from mud-rich facies were sampled using a small handheld wood drill with diamond bit. Larger samples were placed in copper boats for stable isotopic analysis, and excess moisture was removed in a desiccator over a period of 48 hr. Hand-drilled samples were then reacted in a common phosphoric acid bath method at 90°C for 10 min, and a Finnigan-MAT 251 analyzed the produced CO_2. Microdrilled samples were placed in glass vials and reacted in a common phosphoric acid bath at 70°C in a Kiel III device, and a Delta-Plus analyzed the produced CO_2. Data are reported relative to Vienna Peedee belemnite after the standard isobaric corrections were applied. Analytical precision for $\delta^{13}C$ and $\delta^{18}O$ measurements was based on standards and replicates and is ≤ 0.1 ‰ for each.

Microthermometry

Fluid-inclusion analysis was performed by Fluid Inclusion Technologies (FIT), Inc. with a Fluid Inc. modified U.S. Geological Survey heating-freezing stage using standard techniques. Polished petrographic slides were examined in both plane light and under ultraviolet illumination to select appropriate fluid-inclusion populations for quantitative study. Raw $T_{h(aq)}$ (temperature of homogenization of the aqueous phase) are reported without attempts to correct for pressure. This was

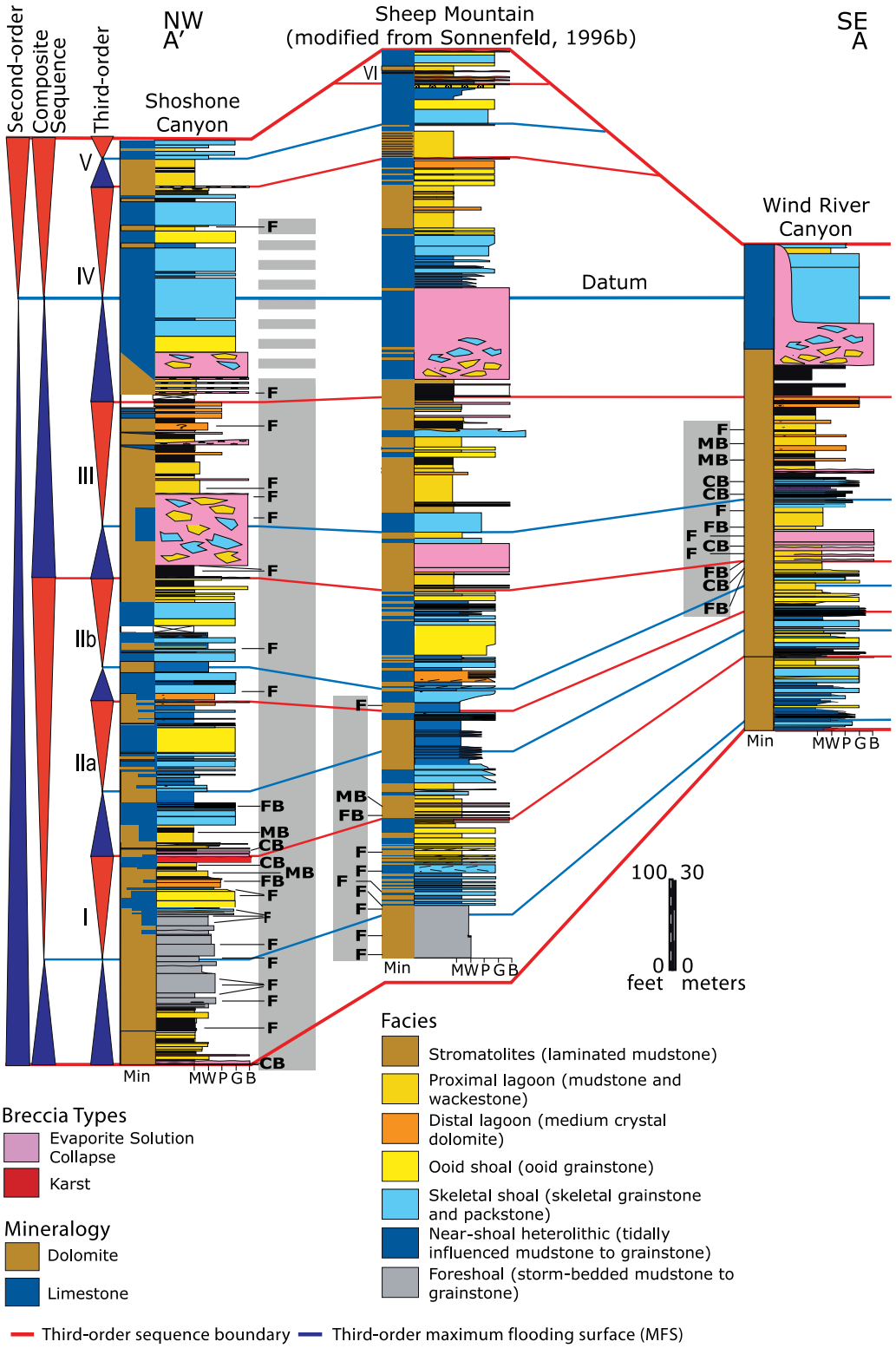

Figure 2. Cross section of measured sections with sequence-stratigraphic interpretations. Late-stage calcite locations from outcrop are highlighted by gray fields and are labeled as F (calcite-filled vertical to subvertical fracture), FB (fracture breccia), MB (mosaic breccia), and CB (chaotic breccia). Tectonic hydrothermal breccias are concentrated in sequences II and III, whereas in the Shoshone Mountain, area fractures occur in the entire section. Min = mineralogy; M = mudstone; W = wackestone; P = packstone; G = grainstone; and B = breccia (modified from Smith et al., 2004).

done because pore pressures are unknown, as are dissolved gas contents, and because empirically, raw $T_{h(aq)}$ commonly provides a reasonable approximation for T_t (trapping temperature) in the sedimentary environment (D. Hall, FIT, 2005, personal communication). Photomicrographs identifying representative aqueous inclusion populations were collected along with a low-magnification photomicrograph for rock description.

Strontium Isotopes

Strontium isotope ratio analysis was performed by the Geosciences Department of the University of Arizona and described in the procedures outlined by Ducea et al. (2002).

GEOLOGIC SETTING

Paleogeographic and Tectonic Setting

The Mississippian Madison Formation was deposited on a shallow-marine carbonate ramp that was located approximately 0–10°N of the paleoequator and extended from the Canadian Arctic to New Mexico, approximately 1600 km (994 mi) long and 400 km (248 mi) wide (Maughan, 1983; McKerrow and Scotese, 1990; Kraus et al., 2004). The ramp proper was bounded to the north by the central Montana trough and Williston Basin, to the west by the Antler highlands, and to the east by the Transcontinental arch (Sando, 1976; Gutschick and Sandberg, 1983; Maughan, 1983). The present-day configuration of Madison outcrops and subsurface reservoirs was achieved during the Late Cretaceous (65–75 Ma) to Eocene (50–55 Ma) Laramide orogeny (Keefer, 1965a, b; Dickinson et al., 1988). The middle Eocene age (43–52 Ma) Absaroka Volcanic Supergroup is evidence for early termination of Laramide deformation in northwest Wyoming (Fritz and Harrison, 1985). The only other igneous activity occurred prior to the Laramide orogeny west of the overthrust belt and along the trend with major Cretaceous batholiths. These batholiths represent the initiation of Laramide deformation during the Maastrichtian (68–78 Ma) and mark the onset of eastward migration of subduction-related magmatism (Dickinson and Snyder, 1978). During the orogeny, the Bighorn and Wind River basins formed and are the focus of this study. Outcrop locations from the margins of the Bighorn Basin are shown on a present-day geologic map (Figure 1) of Montana and Wyoming. The Bighorn Basin is approximately 320 × 80 km (198 × 49 mi) and covers about 26,000 km^2 (10,038 mi^2). This basin is bordered by the Bighorn Mountains in the east, the Absaroka volcanics in the west, the Owl Creek Mountains in central Wyoming, and the Lewis and Clark lineament in southern Montana (Blackstone and Huntoon, 1984). This area was a large intermontane basin that was partitioned by a series of faults and fault-bounded anticlines. Formation of the basin during the Late Cretaceous began in response to loading of the lithosphere, which was accommodated by high-angle reverse faults cored to the basement. The Bighorn Basin has been classified as a ponded basin by Dickinson et al. (1988), meaning that much of the sediment received during the Cenozoic was deposited in lacustrine or marginal alluvial environments. After the Laramide orogeny, the basin was epeirogenically uplifted to its current position, and although the highest peaks now are at approximately 3.5 km (2.1 mi) above sea level, the base of the Paleozoic section lies nearly 3200 m (10,500 ft) below sea level at the basin center (Blackstone and Huntoon, 1984).

Laramide-age structures are typically broad fault-controlled folds ranging from the syncline of the Bighorn Basin to 150–1500-m (492–4921-ft) wavelength anticlinal structures (Blackstone and Huntoon, 1984). The pre-Laramide sedimentary thickness of the basin was about 3.7 km (2.3 mi), of which 670 m (2200 ft) are Paleozoic in age (Blackstone and Huntoon, 1984; Peterson, 1986; Dickinson et al., 1988). Folds were generated by movement along reverse faults attached to the interface between the sediments and the underlying Precambrian basement and are now distributed in a racetrack-type pattern around the edge of the basin. Today, these folds host most of the oil fields of the Bighorn Basin, and estimates of present-day maximum burial of the Madison at the basin center are 6–7 and 5–6 km (3.7–4.3 and 3.1–3.7 mi) near the basin flanks (Dickinson et al., 1988). The outcrops from this study are assumed to have been buried to depths not exceeding the pre-Laramide estimates of 3–4 km (1.8–2.5 mi). The following paragraphs describe the structural style at the sampling locations in the basin. Each site has its unique style that proved to be important for the distribution and the geochemistry of the tectonic-hydrothermal breccias.

Rattlesnake Mountain Anticline: Shoshone Canyon

Rattlesnake Mountain is located 7 km (4.3 mi) west of Cody, Wyoming, and is a basement-cored anticline with a northwest-trending fold axis (Narr, 1993). The Shoshone Canyon region of the anticline, 7 km (4.3 mi) west of Cody, Wyoming, has been described as a backthrust off the Line Creek and Oregon Basin master fault system (Blackstone, 1986; Erslev, 1990). Major faults in the anticline (Figure 3A) are a combination of high-angle (82–84°SW) reactivated pre-Laramide normal faults that are cored in Precambrian pegmatite dikes and Laramide thrust faults (40–80°SW) that

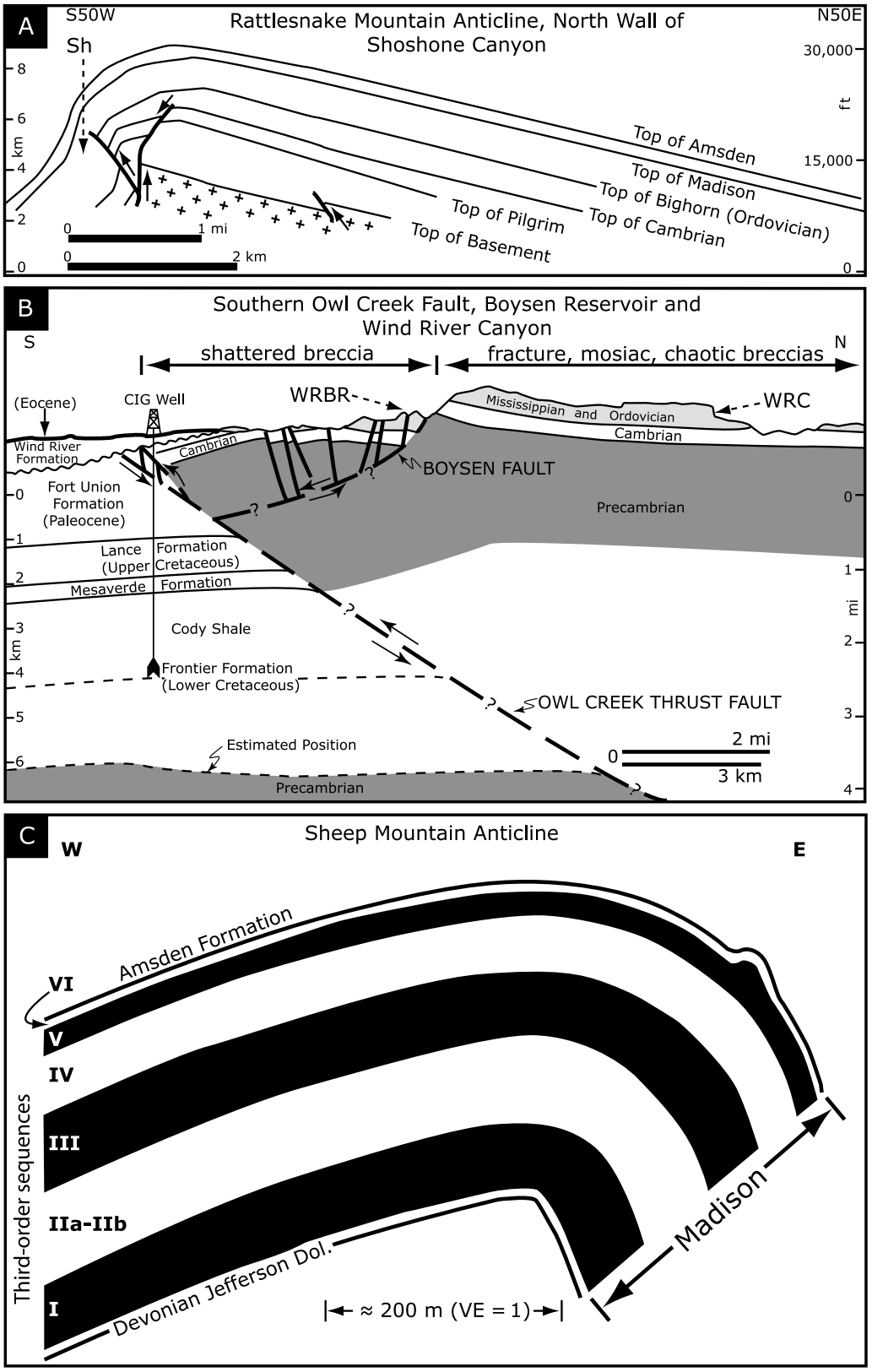

Figure 3. Present-day tectonic and structural setting of field locations investigated in this study. (A) Shoshone Canyon is located in the southwestern limb of the Rattlesnake Mountain anticline, and the measured section (labeled Sh) is close to the frontal edge and deep-rooted fault (modified from Erslev, 1990). (B) The Wind River Canyon section (labeled WRC) is located in the hanging wall of the Owl Creek thrust sheet, whereas the Wind River Boysen reservoir section (labeled WRBR) is located at the tip of the Owl Creek thrust sheet in the isostatically collapsed zone (modified from Blackstone, 1988). Horizontal arrows represent the occurrence of the different types of tectonic breccias in the Wind River Canyon area. (C) The Sheep Mountain anticline is an asymmetric basement fault cored and northwest-southeast–trending anticline (Sonnenfeld, 1996b). Refer to Figure 2 for measured sections in A, B, and C.

formed in response to uplift of the basement-cored backthrust (Erslev, 1990). The absence of basement folding and lack of rotation in pegmatite dikes indicate that the basement acted as a nonrotational and rigid block (Stearns, 1970; Erslev and Rogers, 1993; Narr, 1993). The Shoshone Canyon stratigraphic section (Figure 3A) from this study is located to the southwest of the folded sedimentary rocks in the region above the basement-cored normal fault; these strata are in fault contact with the basement (Narr, 1993).

Eastern Owl Creek Mountains: Boysen Reservoir and Wind River Canyon

Major uplift and folding of the Precambrian basement, eastern Owl Creek Mountains, did not occur until the Paleocene to Eocene (Keefer, 1965a, b; Paylor and Lang, 1990); these rocks now override the northern edge of the Wind River Basin along the east-striking South Owl Creek Mountains thrust fault (Keefer, 1970) and are responsible for approximately 9000 m (29,500 ft) of structural relief on the basement surface (Paylor and Lang, 1990). Seismic data interpretation indicates that the fault dips gently to the north and accommodates approximately 16 km of basement overhang (Gries, 1983). In this study, the tectonic-hydrothermal breccias from the Wind River Canyon were derived from the hanging-wall block of the South Owl Creek Mountain thrust fault and have been interpreted to have formed during episodes of Laramide thrusting. Core data from the Madden Deep field and the CIG exploration well, including field evidence from the Boysen State Park area, document a complex east-striking fault zone that has been interpreted to have formed from isostatic collapse of the uplifted hanging wall (Sales, 1983). The most intensely deformed tectonic-hydrothermal breccias, shattered breccias from above the Boysen reservoir, are located in this region of the thrust sheet, where high-angle rotational faults mark the north and south boundaries of the uplift (Figure 3B).

Sheep Mountain Anticline

Sheep Mountain anticline is a Laramide-age doubly plunging anticline (Savage and Cooke, 2004). This asymmetric basement fault-cored and northwest-southeast–trending anticline (Figure 3C) (Bellahsen et al., 2004) is located within the northern Bighorn Basin, Rocky Mountain foreland, Wyoming. The geometry of the fold has been interpreted to have developed early during the Laramide and is constrained primarily by the underlying thrust fault (Bellahsen et al., 2004; Savage and Cooke, 2004). Field data suggest that the deformation of the anticline was expressed regionally by a pre-Laramide compressional fracture set (striking N110°E) and a joint set (striking N45°E) associated with northeast Laramide compression, which is oriented perpendicular to the strike of the fold and is present in the nose, hinge, and backlimb of the anticline (Bellahsen et al., 2004). A third set of joints (striking N135°E) is found only in the hinge of the fold and formed in response to bending, followed by a final set of fractures in the forelimb and backlimb that is interpreted to have formed via the reactivation of old fracture sets in response to thrusting (Bellahsen et al., 2004). The Sheep Mountain stratigraphic section was described from both limbs of the anticline (Figure 3C) (Sonnenfeld, 1996b).

STRATIGRAPHIC SETTING AND DISTRIBUTION OF RESERVOIR-QUALITY DOLOMITE

The Madison Formation is generally composed of dolomite and limestone, but is argillaceous near the base in the basinward sections, and has two regional evaporite solution collapse breccias near the top of the formation. These solution collapse breccias have been used as a lateral correlation tool over hundreds of kilometers into the undissolved evaporites of the Williston Basin (Middleton, 1961; Roberts, 1966; Smith et al., 2004). Karst features characterize the top of the Madison and its internal sequences and cycle tops, suggesting that the Madison was exposed intermittently. The Madison Formation is overlain by the Amsden sandstone, which ranges in age from the late Mississippian to the early Pennsylvanian (Sando et al., 1975). The contact between the Madison and the Amsden is a second-order supersequence boundary that can be correlated throughout the Rockies (Rose, 1976). Internally, the Madison Formation is a second-order supersequence that is composed of two composite sequences, six third-order sequences, and numerous higher frequency cycles (Figure 2) (Sonnenfeld 1996a, b; Smith et al., 2004). The first composite sequence is equivalent to the Lodgepole Formation in the distal part of the ramp and was deposited during the Kinderhookian to the lower Osagean (Elrick, 1990; Sonnenfeld, 1996a, b; Buoniconti, 2006). The Lodgepole Formation records a major progradational package of shallow-marine carbonate

sediments. The younger composite sequence (largely the Mission Canyon Formation in the distal part of the ramp; Buoniconti, 2006) represents a major change in carbonate depositional profiles from homoclinal ramp to flat-topped shelf, which was deposited during the lower Osagean to lower Meramecian (Buoniconti, 2006). At its base, this composite sequence is a laterally expansive deposit of restricted lagoonal facies that are capped by regionally extensive grainstone deposits. The evolution from ramp to flat-topped shelf was likely driven by the long-term eustatic rise in sea level, which may reflect variations in backbulge subsidence rates in the Antler foreland basin (Sonnenfeld, 1996a).

Individual third-order sequences of the Madison Limestone are approximately 2 m.y. in duration and are referred to as sequences I to VI by Sonnenfeld (1996a, b) and Smith et al. (2004). Elrick (1990) departs from this scheme as she subdivides sequence II into two third-order sequences in northwestern Wyoming and southwestern Montana. Katz et al. (2005) provide further evidence that this subdivision is justified because a positive carbon isotope excursion in sequence II returns to minimum values at the additional sequence boundary (Figure 2; sequence IIa), indicating that the transgressive hemicycle is approaching an accommodation minimum. Consequently, sequence II is here divided into two sequences, referred to as sequences IIa and IIb (Figure 2).

The main reservoirs of the Madison Formation occur in mud-dominated early dolomites that are most commonly found in the transgressive parts of the sequences and cycles. Downdip on the ramp, more than 90% of the mud-dominated facies and less than 5% of the grain-dominated facies were dolomitized by fabric-selective dolomite (Smith et al., 2004). Reservoir-quality dolomite from all rock types, however, occurs in the middle part of the ramp (Smith et al., 2004). All rock types are pervasively dolomitized in middle-ramp parts of the second-order supersequence transgressive systems tract. Here, the rock fabric exerted little control over dolomitization because 70% of the grainstones and 50% of the mudstones were dolomitized, but dolomitized grainstones have generally higher permeability-to-porosity ratios (Smith et al., 2004).

BRECCIAS IN THE MADISON FORMATION

Four major breccia types are present in the Madison Formation: surficial karst, evaporite solution collapse, intrusive karst, and tectonic-hydrothermal breccias. Surficial karst and evaporite solution collapse breccias are an important part of the sequence-stratigraphic framework, whereas penetrative karst breccias and tectonic breccias cut across stratigraphy.

Darkened Chaotic Breccia with Dolomite Matrix (Surficial Karst)

Within the Madison Formation, surficial karst breccias occur at the tops of sequences I, IV, and V and are 1 cm (0.4 in.) to several meters thick. They typically have a micritic or argillaceous matrix. The clasts in these breccias are commonly darkened (Figure 4A) relative to the clasts in other breccia types. These breccias mark sequence boundaries and generally do not cut across bed boundaries (Smith et al., 2004). These breccias are interpreted to have formed during periods of prolonged exposure through wetting and drying and rooting of exposed carbonates. Interestingly, surficial karst is not present in all sequences of the Madison Formation, indicating that it did not form or that it was removed during the next transgression.

Chaotic Breccia with Argillaceous Dolomite Matrix (Evaporite Solution Collapse Breccias)

This polymict breccia type ranges from centimeters to tens of meters thick and is composed of millimeter- to meter-size clasts of dolomite and limestone (Figure 4B). Most of the breccias form beds with irregular tops and planar bases, but some breccias form in small patches within lagoonal mudstone. Clasts have angular shapes and range in size from coarse sand to large boulder. The matrix of most of the breccias is argillaceous dolomite (Figure 4C) with higher gamma-ray values than the surrounding dolomite and limestone.

These breccias are located predominantly at the base of sequences III and IV and are interpreted as the collapse of a lithified formation into solution cavities or by the dissolution of thick and massive beds of evaporites and the collapse of overlying and intercalated strata into the voids during second-order emergence in the late Mississippian (Keefer and Lieu, 1966; Sando, 1967; Moore, 1995; Sonnenfeld, 1996a, b; Smith et al., 2004). The solution collapse breccias present in outcrop and core throughout Wyoming and Montana are time equivalent to deeper water strata of the winnowed and reworked Delle phosphatic member in Idaho, Utah, and Nevada (Sandberg and Gutschick, 1984; Nichols and Silberling, 1991; Silberling et al., 1997; Jewell et al., 2000).

Typical collapse breccia profiles include a lower interval of laminated or structureless mudstone interbedded

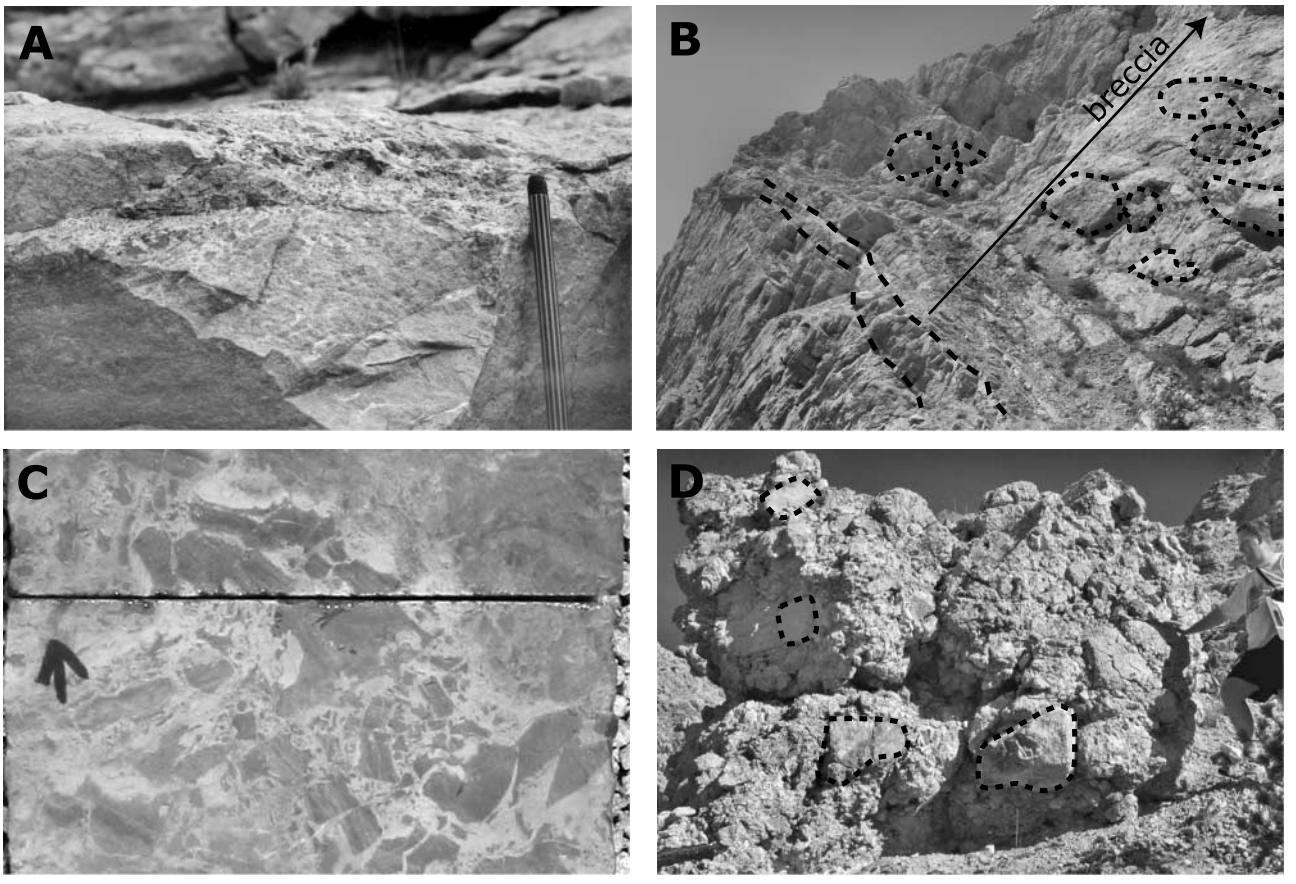

Figure 4. Examples of breccias in the Madison Formation. (A) Surficial karst or exposure-related breccia. These breccias are commonly 1 cm (0.4 in.) to several meters thick and have a micritic or argillaceous matrix with darkened clasts. These breccias mark sequence boundaries and generally do not cut across bed boundaries (Shoshone Canyon, sequence I). Pen in the lower right is for scale. (B) Stratiform breccia with submeter- to meter-wide rounded clasts. This breccia is cemented by coarse isopachous calcite and predominantly by argillaceous dolomite matrix. It has been interpreted as an evaporite solution collapse breccia (highlighted 1-m [3.3-ft]-thick bed for scale; base of sequence IV, Sheep Mountain anticline). Outlined clasts are limestone. (C) Breccia with dolomite matrix and dolomitized breccia clasts and has been interpreted as an evaporite solution collapse breccia. Width of core is 3 in. (7.6 cm) for scale (base of sequence III, Church Buttes 31 core at 5622 m [18,444 ft], Wind River Basin). (D) Intrusive karst-pipe breccia filled with rounded to angular clasts of limestone, dolostones, and sandstone (outlined clasts) in a largely siliciclastic matrix. Pipe is 5 m (16 ft) in diameter and penetrates 75 m (246 ft) from the top of the Madison Limestone (Wind River Canyon sequence III).

with nodular or thin-bedded breccias. The overlying collapse zone typically has smaller clasts at the base that coarsen upward to cobble- and boulder-size clasts (Sando, 1974, 1988). Rounded clasts were likely transported some distance, suggesting pronounced fluid flow in the collapse zones. The occurrence of these breccias extends over thousands of square miles in outcrop and core along stratigraphic horizons and has been used by Sonnenfeld (1996a) and Smith et al. (2004) as correlation horizons between sections. These two solution collapse breccias also have been correlated to thick (up to 30 m [100 ft]) undissolved evaporite in the subsurface of the Williston Basin (Middleton, 1961; Roberts, 1966).

Chaotic Breccia with Siliciclastic Matrix or Associated Siliciclastics (Intrusive Karst Breccia)

This type of breccia differs from collapse breccias and surficial karst breccias in that it commonly occurs in pipes or sinkholes that cut down into the Madison Formation (Figure 4D). The chaotic breccias that infill these cavities typically have a characteristic yellow to reddish silty matrix and a polymictic composition (massive mudstones, laminated mudstones, and chert). This breccia is interpreted as intrusive karst breccia that developed after the deposition of the Madison Formation in conjunction with a widespread middle Meramecian unconformity that was later onlapped by

nonmarine and estuarine facies of the Amsden Formation (Sando, 1988). The hiatus associated with this vast karst plain ranges from 5 to 34 m.y. along the Transcontinental arch and is conformable in areas of Montana, Idaho, and Utah (Sando et al., 1985; Sando, 1988; Reid, 1991). Ettenshohn (1993) postulates that this unconformity represents the last epeirogenic pulse related to the Antler orogeny.

Calcite-Cemented Breccias and Fractures (Tectonic-Hydrothermal Breccia)

A variety of calcite-cemented breccias occur in the Madison Formation. These breccias crosscut stratigraphy, intruding the formation in a dikelike fashion. In places, they form vertical breccia and fracture corridors; in others, they follow the bedding for short distances before cutting to higher levels. The clasts of the breccia are always angular clasts of the surrounding strata. No matrix is present, but intense cementation by calcite encases the clasts or fills the fractures. Furthermore, the style of brecciation indicates a sudden, explosive genesis from migrating fluids. These breccias are the focus of this study and are described in detail below.

TYPES AND DISTRIBUTION OF THE TECTONIC-HYDROTHERMAL BRECCIAS

Hydrothermal breccias from the Owl Creek thrust sheet are classified into four categories based on fracture density, calcite volume, and clast orientation (Kislak et al., 2001). Fracture breccia contains unrotated clasts and less than 5% late-stage calcite cement (Figure 5A, B). Mosaic breccia contains rotated clasts that are easily fitted together and less than 20% late-stage calcite cement (Figure 5C, D). Chaotic breccia contains rotated clasts and as much as 80% late-stage calcite cement (Figure 5E, F). Shattered breccia has a high fracture density and less than 5% late-stage calcite cement (Figure 5G, H). In the Wind River Canyon and Boysen State Park area (Figure 1), shattered breccias are randomly cut by large (5–10-cm; 2–4-in.) late-stage calcite veins.

Distribution of breccia types at individual outcrops is random. At the regional scale, shattered breccias dominate the leading edge of the Owl Creek thrust sheet (Kislak et al., 2001). These breccias are located in the eastern Owl Creek Mountains, above the western margin of Boysen reservoir. Farther north, away from the leading edge of the thrust sheet, deformation is less intense, and breccia types are predominantly fracture, mosaic, and chaotic.

Sequences I–III in the Wind River Canyon are pervasively dolomitized by partially replacive dolomite (5–75 μm wide), whereas sequence IV is limestone (Smith et al., 2004). Sequences I–III contain ubiquitous examples of fracture, mosaic, and chaotic breccias. These breccias terminate at and penetrate bedding planes and the host rock consists dominantly of lower porosity (less than 10%) dolomitized wackestones and packstones (Figure 5A, C). Figure 6 is a schematic illustration of a late-stage calcite-cemented breccia from sequence III, showing that fracture breccias dominate porous foreshoal (burrowed and dolomitized wackestones) and near-shoal heterolithic (tidally influenced and dolomitized skeletal peloidal wackestones to packstones) facies, whereas mosaic and chaotic breccias dominate nonporous shallow intertidal (dolomitized mudstones) and proximal lagoonal (dolomitized peloidal skeletal mudstones to wackestones) facies. In this example, brecciation of the host rock occurs in all facies as described by Smith et al. (2004).

At Sheep Mountain anticline (Figure 2), porous (15–25%) dolomite mudstones and wackestones contain vertical to subvertical fractures and fracture swarms in sequences I and II (Smith et al., 2004). Cementation halos of up to 2 cm (0.8 in.) around the fracture indicate that late-stage calcite-bearing fluids penetrated and cemented preexisting permeability pathways (Figure 7A). Fracture breccias also overprint well-cemented and thin solution collapse breccias at the base of sequence II, Sheep Mountain anticline.

Sequence I–III, Shoshone Canyon, are dominated by tectonic-hydrothermal fractures in a wackestone host rock except for a chaotic breccia at the base of the section. In sequence I at Shoshone Canyon, parallel sets of vertical fractures filled with late-stage calcite penetrate dolomite mud to wackestones (Figure 7B). Fracture breccias also overprint the sequence III dissolution collapse breccia; however, these are not common. Only two hydrothermal fractures were found in sequence IV. Otherwise, the fractures and breccias terminate near or at the boundary of sequences III and IV.

The best example of shattered breccias is located just past the southern entrance to Wind River Canyon in the eastern Owl Creek Mountains, western margin of Boysen reservoir from Interstate 20. Here, sequences II and III are shattered by dolomitized breccias that are crosscut by a later stage of large (5–10-cm; 2–4-in.) and small (<5-cm; <2 in.) late-stage calcite veins, suggesting that the dolomite may have developed early

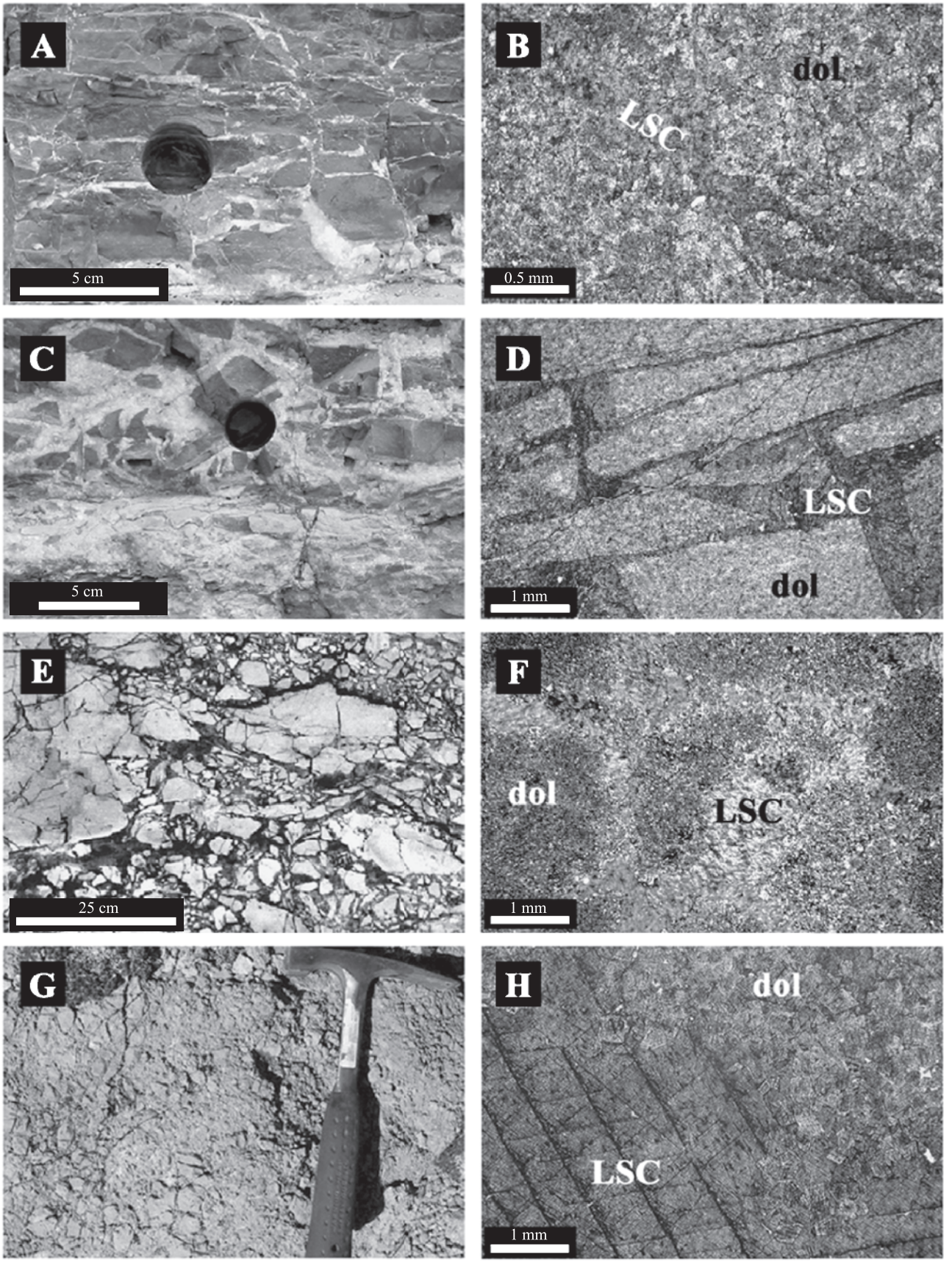
A
5 cm
B
dol
LSC
0.5 mm
C
5 cm
D
LSC
dol
1 mm
E
25 cm
F
dol
LSC
1 mm
G
H
dol
LSC
1 mm

during the Laramide orogeny in the Late Cretaceous (Keefer, 1965a, b). The breccia clasts are composed of 100% coarsely crystalline, non-fabric-selective, and replacive dolomite, 200–500 μm wide (Figure 5H).

EARLY- AND LATE-STAGE DIAGENETIC FEATURES IN THE MADISON FORMATION

Samples for this study were collected with the aim of distinguishing the geochemical and petrographic attributes of late-stage calcite-cemented breccias and fractures from other diagenetic manifestations occurring in the Madison Formation. Dolomite samples and nonrecrystallized marine calcites were analyzed petrographically and chemically to distinguish the host or wall rock from the late-stage calcite-cemented breccias and fractures. These samples include (1) finely crystalline (5–75-μm-wide) fabric-selective dolomite from mud-rich facies (Figure 8A); (2) medium-crystalline (75–200-μm-wide) non-fabric-selective and partially fabric-destructive dolomite from wackestones, packstones, and grainstones (Figure 8B); (3) a range of calcites from ooid, mixed skeletal-oolitic (Figure 8C), and skeletal grainstones, packstones, and wackestones; and (4) partially micritized ooids in an ooid grainstone cemented by early-marine fibrous isopachous calcite (Figure 8D).

We sampled meteoric calcite of Mississippian age from microkarst, a pisolitic packstone, and an ooid grainstone, as well as meteoric calcite of Laramide to modern age from a speleothem deposit to document geochemical differences between sparry calcite samples of Mississippian and later meteoric origins. The purpose of collecting these samples was to provide constraints for understanding the source of the tectonic-hydrothermal late-stage calcite-bearing fluids as compared to samples with depleted and possibly meteoric calcite values with similar $\delta^{18}O$ values. The first three varieties are of Mississippian age and of interpreted meteoric origin for the following reasons. The first variety is an oolitic grainstone (Figure 9A) with rip-up clasts cemented first by fibrous isopachous marine calcite followed by a second generation of interparticle sparry meteoric calcite typical of early near-surface diagenesis (James and Choquette, 1983; Scholle and Ulmer-Scholle, 2003). The rip-up clasts are fragments of cemented crusts that were lithified early and then eroded and redeposited into intertidal-subtidal oolitic sands. The second variety is what is interpreted as microkarst (Figure 9B). It commonly occurs at the tops of genetic cycles in the Madison Formation and has an irregular erosional surface that extends a few centimeters to 0.5 m (1.6 ft) into the underlying bed. In outcrop, these are thin and laterally discontinuous and are commonly iron stained. Internally, they are composed of subrounded to angular centimeter-size breccia clasts in a matrix of gray limestone. The karst is always overlain by subtidal facies interpreted as the next transgressive phase. This is distinctly different from cave collapse features or large, penetrative karst systems in that in microkarst, the bottom erosive contact does not penetrate through the underlying cycle. The third variety is an iron-stained pisolitic packstone with geopetal structures and fenestrae occluded by sparry calcite cements (Figure 9C) and likely formed as part of an island complex exposed to the vadose environment (Burke, 1994; Petty, 1996). Variety 4 is a speleothem deposit (Figure 9D) from southwest Montana, which formed as a result of Laramide uplift of the Rocky Mountains. This sample was collected to represent local meteoric effects on oxygen isotope fractionation at higher latitudes and orographic settings compared to the equatorial setting of the Mississippian (varieties 1–3).

RESULTS

Stable C and O Isotopes

Stable isotope analysis of $\delta^{18}O$ and $\delta^{13}C$ was used to distinguish Madison carbonates from late-stage calcite (Figures 10, 11). Samples were first categorized by

Figure 5. Field photographs and thin-section photomicrographs of the four types of tectonic-hydrothermal breccias identified in the Madison Formation. The breccias are monomict with clasts coming from the adjacent host rock. The breccias have no matrix but are always cemented by calcite. (A) Fracture breccia that has unrotated clasts and less than 5% late-stage calcite cement (LSC). (B) Thin-section photomicrograph of fractured dolomite with calcite as fracture filling. (C) Mosaic breccia that contains rotated clasts that are easily fitted together and have less than 20% calcite cement. (D) Thin-section photomicrograph of the mosaic breccia. (E) The chaotic breccia contains rotated clasts and as much as 80% calcite cement. (F) Thin-section photomicrograph of the chaotic breccia. (G) In the shattered breccia, the fracture density is extremely high, clasts do not fit, but the calcite cement is less than 5% of the rock volume. This breccia type only occurs in Boysen State Park, the frontal part of the Owl Creek thrust sheet. (H) Thin-section photomicrograph of the shattered breccia. Note that in all photomicrographs, the calcite cement occludes all porosity around breccia clasts. dol = dolomite.

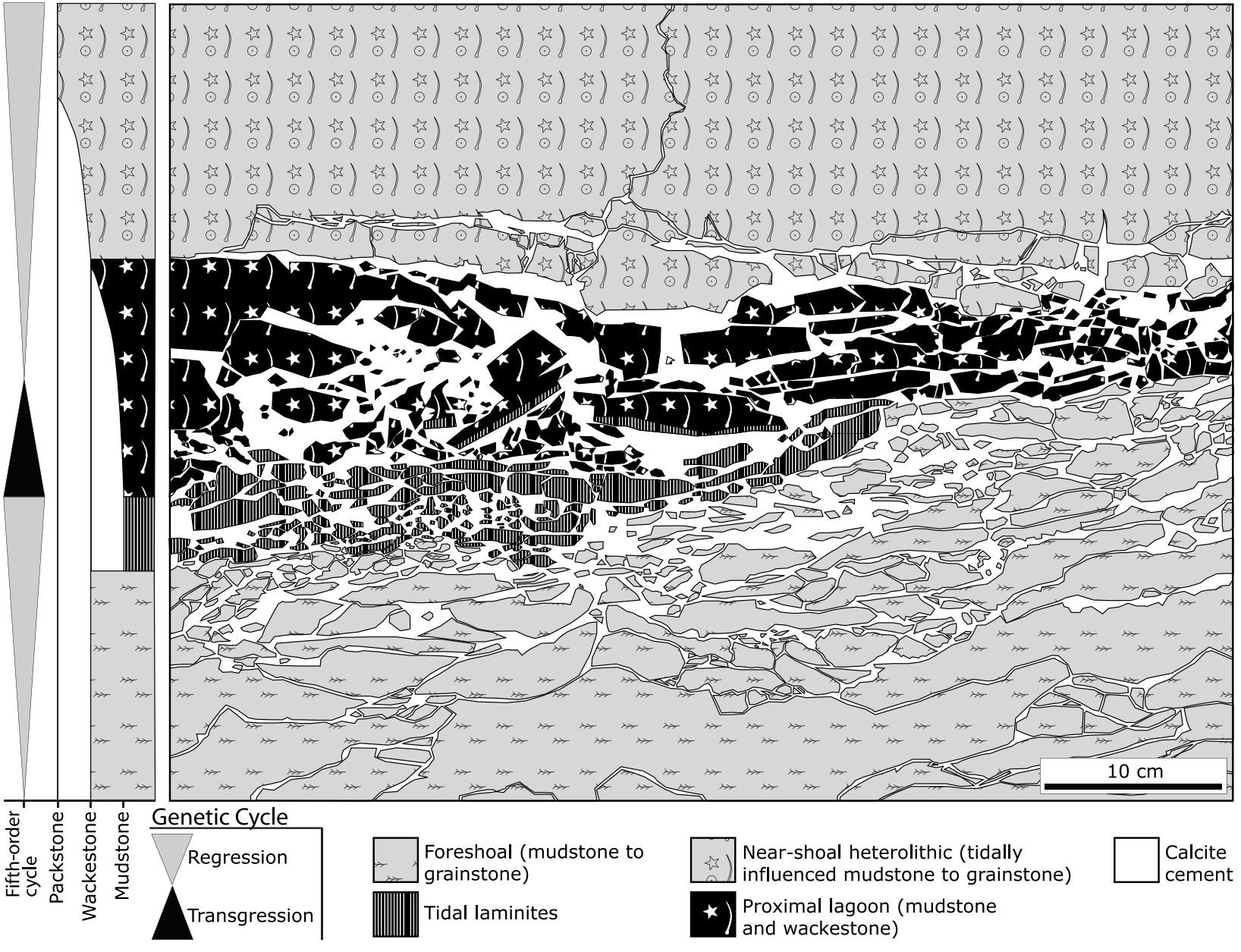

Figure 6. Schematic illustration of a calcite-cemented breccia based on a section from Wind River Canyon, sequence III. Brecciation of the host rock occurs in all facies as described by Smith et al. (2004).

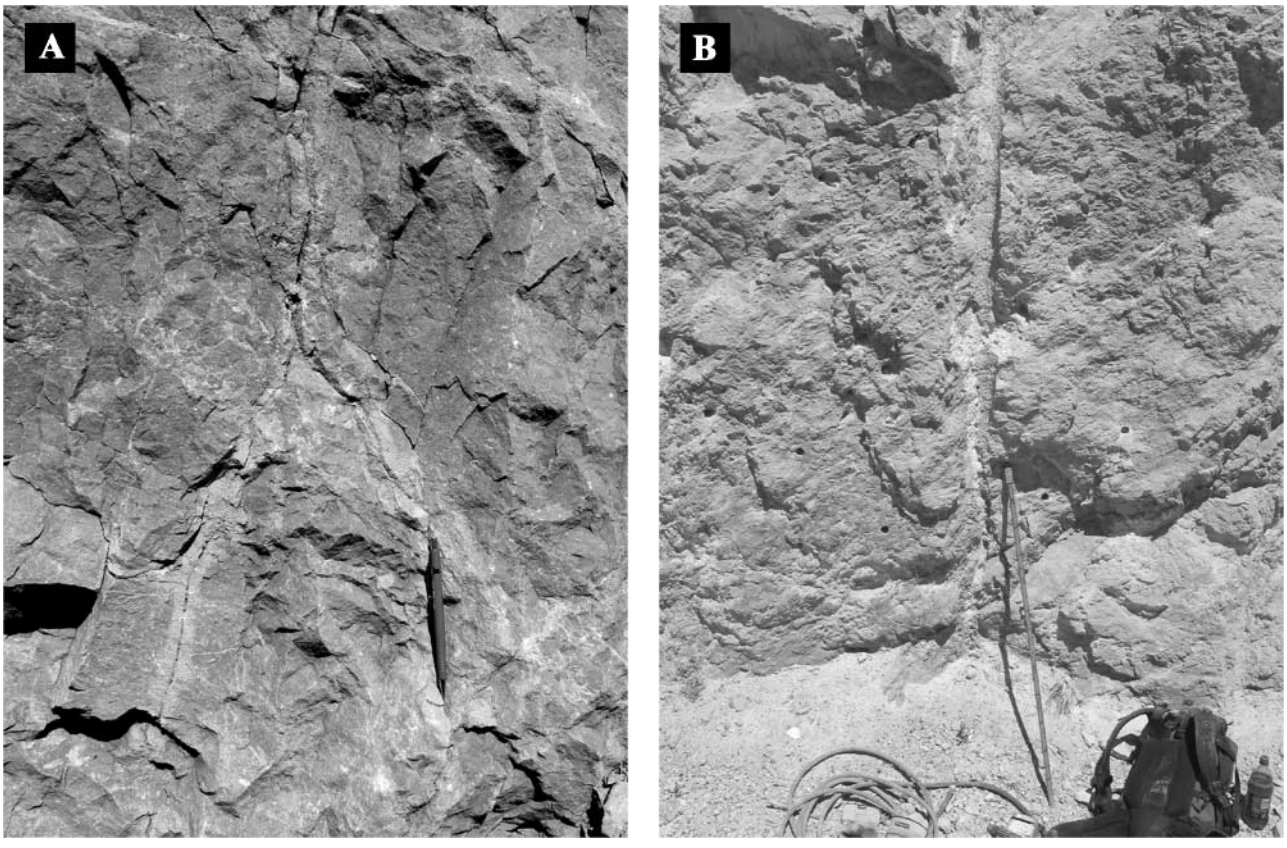

Figure 7. Field photographs of vertical to subvertical and splayed fractures with cementation halos showing penetration of late-stage calcite-bearing fluids into porous dolomite host rock. (A) Cementation by late-stage calcite up to 2 cm (0.8 in.) away from the fracture (sequence I, Sheep Mountain anticline). (B) One of several parallel sets of vertical fractures, sequence I, Shoshone Canyon. Staff is 1 m (3.3 ft) for scale.

facies according to Smith et al. (2004) and then screened petrographically to determine diagenesis prior to isotopic analysis. The stable isotopic composition of the late-stage calcite of each location shows a slightly different signature. Late-stage calcite cements (n = 125) have the most depleted $\delta^{18}O$ values (-26.5 to -15.1 ‰) and the widest range of $\delta^{13}C$ values (-7.8–11.5 ‰) documented in this study (Figure 10). Late-stage calcites from Shoshone Canyon (n = 55, Figure 11) have the greatest range in $\delta^{18}O$ (-26.5 to -15.3 ‰) and the least range in $\delta^{13}C$ (-2.6–1.6 ‰) values measured from all late-stage calcite samples. Late-stage calcites from Wind River Canyon (n = 42, Figure 11) share a similar range in $\delta^{18}O$ (-22.0 to -15.1 ‰) and $\delta^{13}C$ (-4.2–0.4 ‰) values as Shoshone Canyon. Boysen reservoir late-stage calcites (n = 6, Figure 11) have the narrowest range in $\delta^{18}O$ (-18.0 to -16.6 ‰) and most enriched $\delta^{13}C$ (4.6–11.5 ‰) values for all calcites. Late-stage calcites from Sheep Mountain anticline (n = 22, Figure 11) have $\delta^{18}O$ (-22.6 to -15.1 ‰) values similar to the range reported for Wind River Canyon and the most depleted $\delta^{13}C$ (-7.8 to -0.5 ‰) values of all late-stage calcites.

Microdrilling across the late-stage calcites was performed to assess the evolution of the fluid during the precipitation of the calcite. Transects across the calcite cements show relatively little stable isotope variability in individual samples. A late-stage calcite-filled fracture shows a range in $\delta^{18}O$ values from -20.8 to -19.4 ‰ and $\delta^{13}C$ values from -1.3 to -0.4 ‰ (Figure 12A). A late-stage calcite-filled fracture breccia shows a range in $\delta^{18}O$ values from -19.8 to -19.1 ‰ and $\delta^{13}C$ values from -1.3 to -0.7 ‰ (Figure 12B). A late-stage calcite-cemented mosaic breccia shows a range in $\delta^{18}O$ values from -21.3 to -19.5 ‰ and $\delta^{13}C$ values from -1.7 to -0.9 ‰ (Figure 12C).

Stable oxygen isotopic values from the other types of breccias are more enriched than the values from late-stage calcites. Stable oxygen and carbon isotope values from the darkened chaotic breccia with dolomite cement matrix (surficial karst) are -10.7 to -7.0 ‰ and $+0.6$ to $+2.3$ ‰, respectively. The argillaceous

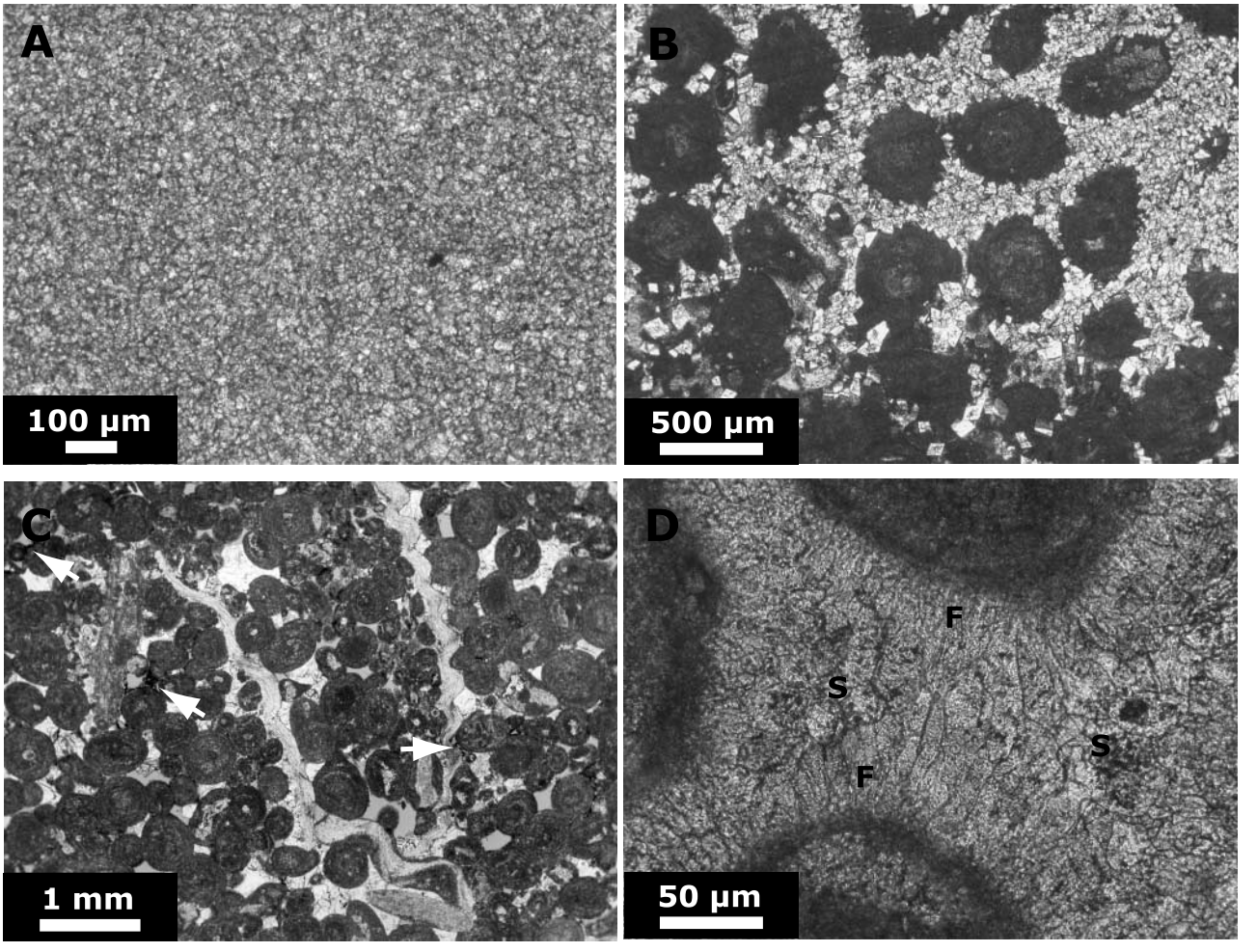

Figure 8. Dolomite (A and B) and limestone (C and D) characteristic of the Madison Formation. (A) Fine crystalline (5–75-µm-wide) dolomite from mud-rich facies, Sheep Mountain anticline, sequence II, 45 m (147 ft). (B) Medium-crystalline (75–200-µm-wide) dolomite crystals that have partially replaced the matrix and the rims of micritized ooids (calcite), Sheep Mountain anticline, sequence I, 22.95 m (75.29 ft). (C) Skeletal oolitic grainstone with minor bitumen staining of interparticle porosity (arrows), Sheep Mountain anticline, sequence I, 30 m (98 ft). (D) Micritized oolitic grainstone with early-marine fibrous isopachous calcite cements (F) around ooids followed by a second generation of interparticle sparry cements (S), Sheep Mountain anticline, sequence II, 80.75 m (264.92 ft).

dolomite matrix from the chaotic breccia (evaporite solution collapse breccia), Bighorn and Green River basins, has $\delta^{18}O$ and $\delta^{13}C$ values from −8.2 to 0.9‰ and 1.1 to 3.2‰, respectively. Where argillaceous dolomite matrix has been replaced by coarse-sparry isopachous calcite, $\delta^{18}O$ and $\delta^{13}C$ values are from −12.7 to −1.9‰ and 0.4 to 2.7‰, respectively.

In comparison, modern speleothems (n = 11) from southwestern Montana were analyzed and have the second most depleted $\delta^{18}O$ values (−17.4 to −16.8‰), which overlap the upper end member of late-stage calcite $\delta^{18}O$ values; $\delta^{13}C$ values for modern speleothems are also depleted (−6.4 to −2.5‰). Mississippian microkarst (n = 1) is composed of depleted $\delta^{18}O$ (−12.7‰) and $\delta^{13}C$ (1.6‰) values; however, this sample is more enriched in ^{18}O than the modern speleothem deposits. Mississippian sparry intergranular calcite (n = 10), which is interpreted to have precipitated in the meteoric environment, has $\delta^{18}O$ (−11.7‰) and $\delta^{13}C$ (1.0‰) values similar to those of the Mississippian microkarst. Sparry calcite (n = 10) cements, filling fenestrae and geopetal structures in an iron-stained pisolitic packstone, also have $\delta^{18}O$ (−11.0‰) and $\delta^{13}C$ (−0.7‰) values similar to the Mississippian meteoric karst and intergranular sparry calcite; the cements in the pisolite packstone are interpreted to have formed during exposure of small islands to meteoric waters. Medium-crystalline, non-fabric-selective to fabric-destructive dolomite and mosaic calcite show a range of $\delta^{18}O$

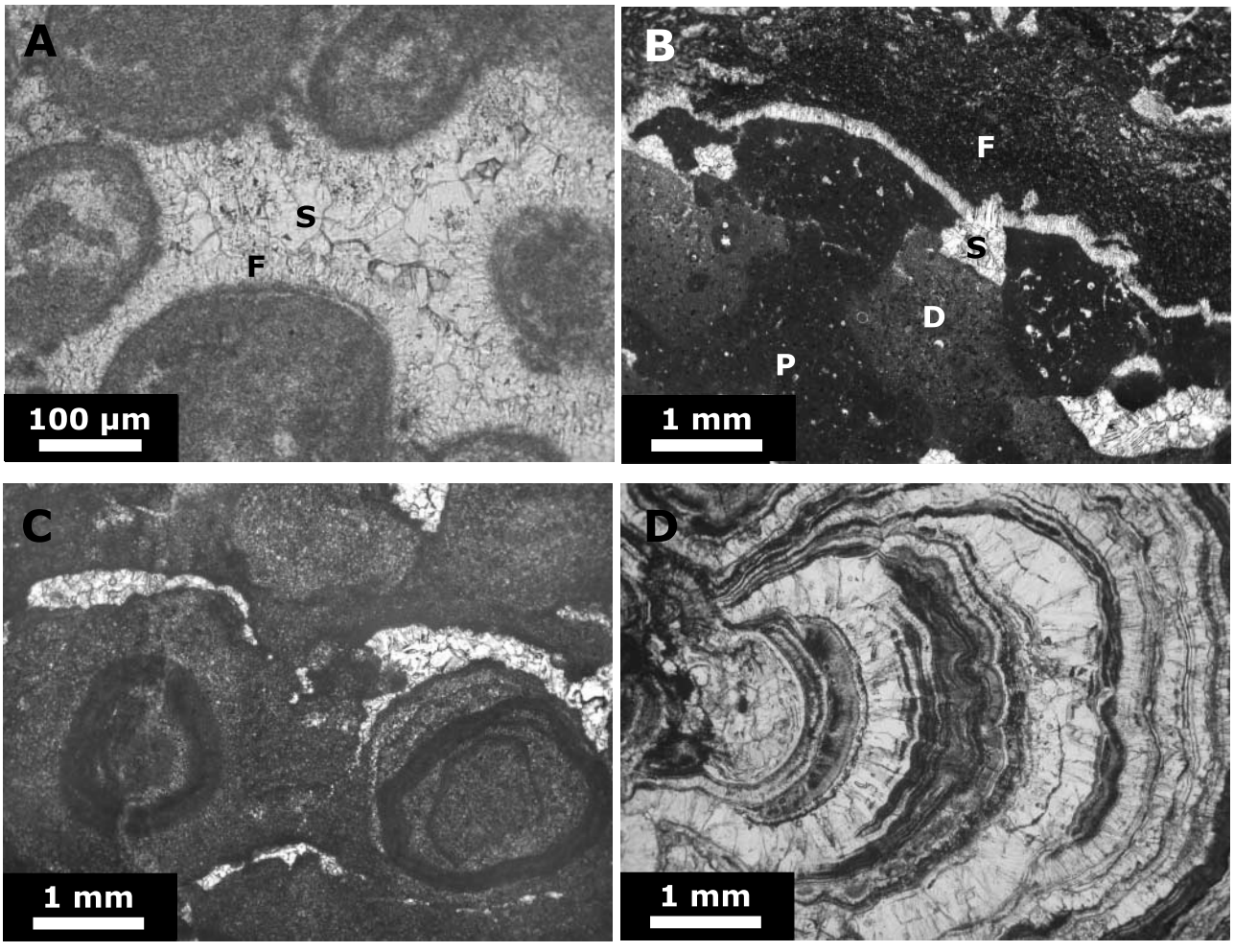

Figure 9. Meteoric calcite from the Mississippian (A–C) and near the time of the Laramide orogeny (D). (A) Oolitic grainstone cemented by fibrous isopachous marine cements (F) around ooids followed by meteoric sparry calcite cementation of the remaining interparticle porosity (S), Sheep Mountain anticline, sequence II, 80.75 m (264.92 ft). (B) Microkarst with an irregular erosional surface highlighted by the throughgoing fibrous calcite cement. This zone of calcite separates the underlying peloidal packstones (P) from the iron-stained ferruginous crust (F) above. Erosional pockets are filled with debris (D) and cemented by sparry geopetal cements (S). This sample is overlain by another erosional surface filled with dark breccia clasts in a matrix of gray limestone (not shown here), southwest Montana, Baldy Mountain sequence II. (C) Iron-stained pisolite packstone with geopetals filled by sparry meteoric cements, southwest-central Montana, 16 Mile Creek sequence III. (D) Speleothem deposit from southwest Montana, Baldy Mountain sequence I.

(−13.0 to −4.8‰) and $\delta^{13}C$ (−1.6–4.8‰) values (Figure 10).

Fine-crystalline and fabric-selective dolomite and primary calcite have $\delta^{18}O$ (−4.8–5.0‰) and $\delta^{13}C$ (−2–7.5‰) values that are more enriched than medium-crystalline, non-fabric-selective to fabric-destructive dolomite, mosaic calcite, and late-stage calcite values from this study (Figure 10) (Veizer et al., 1999). Fibrous isopachous Mississippian marine calcite cement (n = 10) from an ooid grainstone has relatively enriched $\delta^{18}O$ (−2.2‰) and $\delta^{13}C$ (5.5‰) values. Dolomite and calcite wall rock samples with $\delta^{13}C$ values between 3.5 and 7.5‰ are from sequences IIa and IIb and were deposited during the lower Mississippian positive carbon excursion documented by Saltzman et al. (2004) and Katz et al. (2005).

$^{87}Sr/^{86}Sr$ Isotopes

Strontium isotope analysis was used to determine if the fluids responsible for late-stage calcite precipitation interacted with high Rb source rocks such as granites and gneisses. All $^{87}Sr/^{86}Sr$ isotope results are presented in Table 1, along with microthermometric and $\delta^{18}O_{carb}$ and $\delta^{13}C_{carb}$ values. The $\delta^{18}O_{carb}$ values versus $^{87}Sr/^{86}Sr$ ratios are shown in Figure 13.

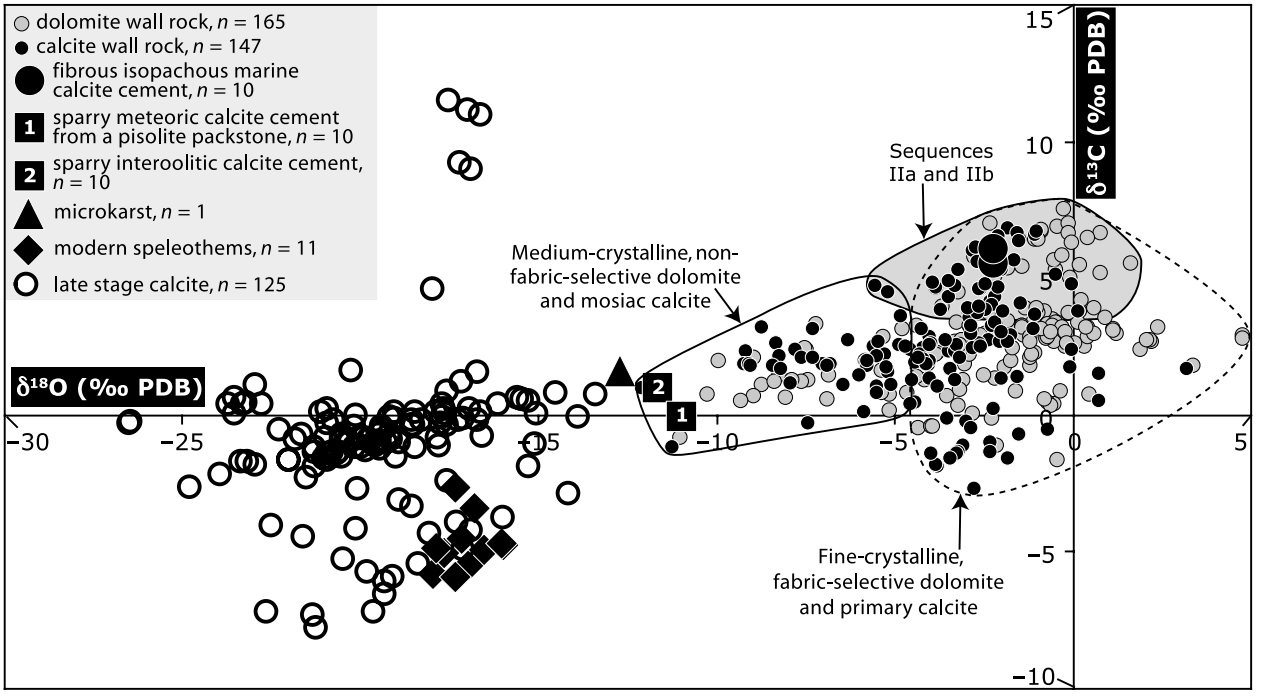

Figure 10. Carbon and oxygen isotope crossplot showing the distribution of carbonate rocks in the Madison Formation. Late-stage calcite samples have the most depleted oxygen isotope values ($\delta^{18}O = -26.5$ to -15.1) of all Madison carbonates, whereas medium-crystalline, non-fabric-selective dolomite and mosaic calcite ($\delta^{18}O = -13$ to -4.8), and fine-crystalline, fabric-selective dolomite and primary calcite ($\delta^{18}O = -4.8$–5) have the most enriched oxygen isotope values. The depletion of the oxygen isotope values in the late-stage calcite indicates precipitation of the calcite from hot fluids. PDB = Peedee belemnite.

Although some isotopic overlap exists between late-stage calcite, burial dolomite, marine dolomite, and ooid grainstones, late-stage calcite has the most radiogenic $^{87}Sr/^{86}Sr$ (0.7089–0.7273) and most depleted $\delta^{18}O$ (-22.8 to -16.6‰) values (Figure 13). Medium-crystalline non-fabric-selective to fabric-destructive dolomite (0.7089–0.7091) is more radiogenic than values reported for Mississippian seawater and less radiogenic than late-stage calcite and coarsely crystalline to non-fabric-selective and zoned dolomite (0.7098).

Strontium isotope ratios of finely crystalline fabric-selective dolomite from mud-rich facies and ooid grainstones (0.7082–0.7083) are the least radiogenic. These samples are within the range of lower Mississippian seawater values (0.7075–0.7085) published by Bruckschen et al., 1999. Therefore, little or no resetting of these samples by diagenetic fluids has occurred.

Microthermometry

Fluid-inclusion analysis was used to determine the minimum entrapment temperature of the fluid responsible for precipitating the host or wall rock surrounding the tectonic-hydrothermal late-stage calcite. All microthermometric results of fluid inclusions from the H_2O-NaCl system are presented in Table 1, along with measured $^{87}Sr/^{86}Sr$ and $\delta^{18}O_{carb}$ and $\delta^{13}C_{carb}$ values. Microthermometric descriptions have been separated into low-temperature fluid inclusions and elevated temperature inclusions (cf. Goldstein and Reynolds, 1994). The hottest entrapment temperatures are from the late-stage calcite and shattered dolomite breccia, which postdate the formation of the rest of the samples in Figure 14.

Reported fluid-inclusion data from dolomites were derived from assemblages of primary inclusions identified by their relationship to the growth zonation of the crystal. Large (10–25-μm-wide) fluid inclusions are common in the late-stage calcite samples, and some have irregular shapes. In these samples, coarse and sparry cements with no clear growth zones contain assemblages of secondary and pseudosecondary inclusions except for one sample (SM 1.95 m [6.39 ft]) that contains metastable primary inclusions indicative of salinities less than 5% NaCl (D. Hall, 2005, personal communication).

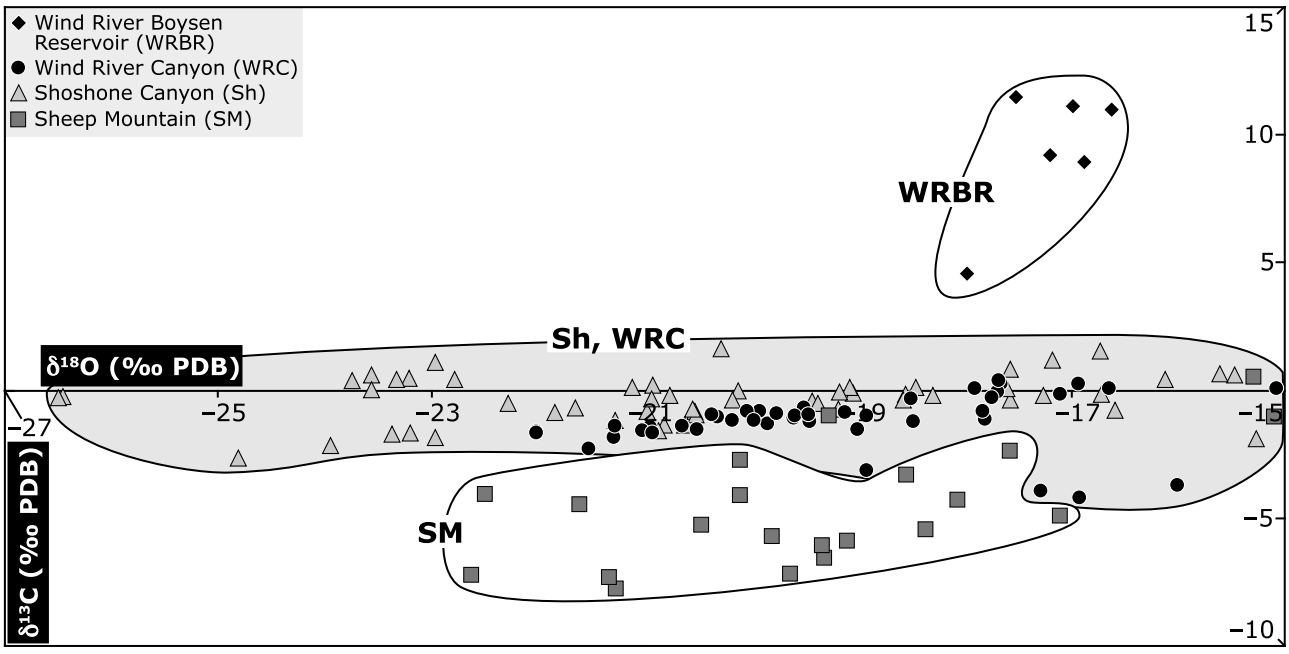

Figure 11. Stable carbon and oxygen isotope crossplot showing the distribution of the late-stage calcites in Figure 10. Boysen reservoir samples are from the shattered breccia at the leading edge of the Owl Creek thrust sheet and have enriched carbon isotope values. Sheep Mountain samples have relatively depleted $\delta^{13}C$ values. Wind River and Shoshone Canyon samples have the greatest range of $\delta^{18}O$ values; Shoshone Canyon samples have the most depleted $\delta^{18}O$ values.

In some samples, stretching of the fluid-inclusion cavities is observed, which initially formed during sedimentation, or different stages of burial diagenesis may have occurred during burial of the Madison Formation to its final depths of 3–4 km (1.8–2.5 mi). Stretching results in elevated homogenization temperatures. During burial, the internal pressure of the inclusion exceeds the surrounding hydrostatic pressure, and the inclusion volume would stretch, or increase, and the density of the inclusion would decrease (Goldstein and Reynolds, 1994).

Low-Temperature Fluid Inclusions

Samples from Sheep Mountain (SM 8.15 m [26.7 ft] and SM 120.6 m [395.6 ft]) and Shoshone Canyon (SH_J; Table 1) have fine-crystalline, fabric-selective dolomite and primary calcite fabrics (Figure 15A–C) and contain low-temperature ($T_{h(aq)}$ range from 45 to 64°C), dominantly monophase and two-phase inclusions. Measured salinities from the sparry calcite (3.4–3.9 wt.% NaCl) in sample SH_J are at or near seawater concentration. However, salinity values (<5–21.9 wt.% NaCl) from fine-crystalline, fabric-selective, and porous stratiform dolowackestones, SM 8.15 m (26.7 ft) and SM 120.6 m (395.6 ft), are the greatest measured in this study. These samples also contain enriched isotopic values ($\delta^{18}O$ = 1–3.1 ‰). Salinity values could not be determined for monophase-liquid inclusions because these could not be artificially stretched. Sheep Mountain dolomites also have low-temperature primary petroleum inclusions (14–64°C). These inclusions fluoresce toward the yellow to white wavelengths, suggesting that the hydrocarbon inclusion has moderate to low gravities and relatively low maturity.

Fluid-inclusion assemblages composed of all-liquid inclusions are diagnostic of the low-temperature phreatic zone environment (Goldstein and Reynolds, 1994), and their $T_{h(aq)}$ is assumed to be less than 65°C as defined in the results from Fluid Inclusion Technologies, Inc., this study. Goldstein and Reynolds (1994) define these inclusions to have formed under conditions less than 50°C.

Elevated Temperature Fluid Inclusions

Three samples, SH_J, WRC 33.65 m (110.4 ft), and WRBR_3a (Table 1), with medium-crystalline replacive dolomite textures (Figure 15C, D), contain elevated temperature ($T_{h(aq)}$ range from 65 to 115°C) gas-liquid fluid inclusions. Sample SH_J consists of replacive, largely unzoned dolomite with minor residual patches of original calcite. Aqueous inclusions in dolomite have homogenization temperatures of

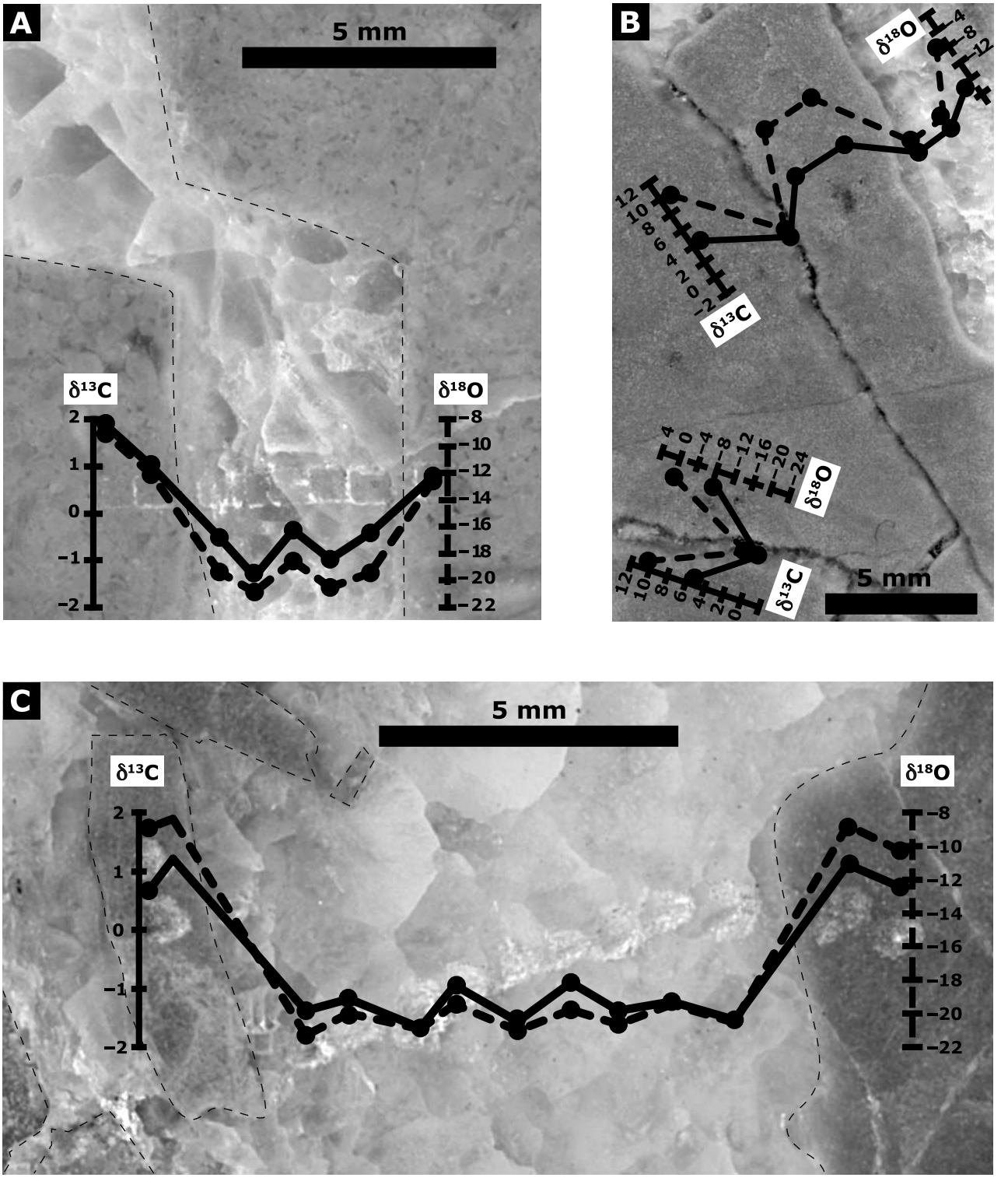

Figure 12. Microdrilled transects through a late-stage calcite cement in fractures and breccias. (A) Cement ($n = 5$) in a fracture from Shoshone Canyon, sequence IIb, 96 m (314 ft). (B) Fracture breccia and cement ($n = 4$) from Wind River Canyon, top of sequence IIa sample P51. (C) Mosaic breccia and cement ($n = 9$) from Wind River Canyon, sequence III sample WR4. Values of $\delta^{18}O$ and $\delta^{13}C$ in the late-stage calcite show very little variability, suggesting that the entire cement formed from the same pool of water and rapidly enough to prevent significant isotopic exchange and temperature change with the fluid or host rock. Solid and dashed lines that connect data points on the isotope graphs represent $\delta^{13}C$ and $\delta^{18}O$ values, respectively.

65–100°C, with most in the 80–100°C range. Salinities range from 0.5 to 6.5 wt.% NaCl, which is low compared with other dolomites from this study. The salinities are somewhat bimodally distributed at 1.0–1.9 and 4.7–6.5 wt.% NaCl.

The zoned dolomite in sample WRC 33.65 m (110.40 ft) is a fabric-destructive dolomite and preferentially occurs between ooid grains and partially penetrates ooid grain margins in a texturally destructive manner (Figure 15D). Aqueous inclusions in this zoned dolomite homogenize at 80–115°C, with a slight bimodal distribution at the 80–90 and 105–115°C range. Cores and rims of this zoned dolomite display the same distribution of homogenization temperatures (80–115°C), and therefore, there is no evidence that dolomite formed during a heating or cooling trend. Salinities of WRC 33.65 m (110.40 ft) are highly variable (7.9–22.0 wt.% NaCl), with most bimodally distributed at 10.2–13.5 and 20.2–22.0 wt.% NaCl. As with temperature, there is no clear core to rim trend, with both modes occurring throughout.

Sample WRBR_3a, from the shattered breccia zone above the Boysen reservoir, Wind River Canyon, contains coarsely crystalline, non-fabric-selective, and zoned dolomite (Figure 5G, H). Aqueous inclusions from the zoned dolomite homogenize at 110–140°C. Cores and rims display the same maximum homogenization temperatures (140°C), but the cores contain a lower minimum temperature (110°C) than the rims (125°C). Salinities in the dolomite are also bimodally distributed. Lower salinities (13.9–14.6 wt.% NaCl) tend to occur in the cores, and higher salinities (21.3–21.7 wt.% NaCl) tend to occur in the rims.

Late-Stage Calcite Fluid Inclusions

Primary inclusions in the late-stage calcite are uncommon because growth zone boundaries are missing in the sparry calcite. Except for SM 1.95 m (6.39 ft), all fluid-inclusion data from the late-stage calcite samples originate from pseudosecondary and secondary inclusion assemblages that were measured along healed fractures and throughgoing fractures and not the sparry calcite, which is the focus of this article. Nevertheless, healed microfractures suggest that fracturing of the primary late-stage calcite was a repetitive process and, therefore, representative of the calcite precipitating within the microfracture.

One sample (SM 1.95 m [6.39 ft]) has primary fluid inclusions, but the sizes ranged from 2 to 20 μm, and some of the larger inclusions contained irregular shapes. Nevertheless, more than 90% of all measured inclusions from SM 1.95 m (6.39 ft) fall within a 20°C $T_{h(aq)}$ range, indicating that they are good estimates of the minimum entrapment temperatures for the late-stage calcite. This late-stage calcite cement (Figure 15E) contains elevated temperature gas-liquid fluid inclusions with the hottest temperatures of homogenization ($T_{h(aq)}$ range from 120 to 140°C). Quantitative salinity measurements are not possible because the inclusions exhibit metastable ice melting, which is most common in inclusions with salinities less than 5 wt.% NaCl (D. Hall, FIT, 2005, personal communication).

SM 1.95 m (6.39 ft) and SM 4 m (13 ft), have secondary and pseudosecondary petroleum inclusions along microfractures and healed microfractures (Table 1), indicating that hydrocarbon migration occurred slightly after the brecciation event during fracturing of the calcite. The petroleum inclusions have low to elevated temperatures (46–85°C). Similarly as in the dolomites, these hydrocarbon inclusions fluoresce toward the yellow to white wavelengths, suggesting the low gravities and relatively low maturity.

DISCUSSION

The geochemical data indicate that a variety of fluids having freshwater to hypersaline compositions over a wide temperature range affected the Madison Formation during diagenesis. The late-stage calcites are distinct from the surrounding host rock and other types of breccias, and our data provide strong evidence that the fluids responsible for precipitating the late-stage calcite migrated from the meteoric environment into the subsurface and were finally reinjected vertically back into the Madison Formation along the basin-bounding and basement-cored faults. The result of this cycle is a void-filling, coarsely crystalline calcite cement that lacks definitive growth zonation with relatively low salinities. These cements have the most depleted $\delta^{18}O$ values, the most radiogenic Sr isotope ratios, and the highest temperatures measured in this study. According to the definition from White (1957) and Machel and Lonne (2002), these cements are hydrothermal in origin.

Below, we discuss the paragenesis from the oldest to the youngest diagenetic environment and will address the diagenetic environment for all carbonate samples used in this study to constrain the hydrothermal origins of the late-stage calcite.

Table 1. Geochemistry of Samples Selected for Fluid Inclusion and Strontium Isotope Analysis*

Sample**	Petrographic Description and Notes	Population***	Number of Inclusions Measured	$T_{h(aq)}$† (°C)	$T_{m(aq)}$†† (°C)	Salinity (wt.%)‡	Bulk Sample $^{87}Sr/^{86}Sr$	Inorganic Carbonate $\delta^{18}O$ (‰ PDB)	Inorganic Carbonate $\delta^{13}C$ (‰ PDB)
SM 8.15 m	Fine-crystalline, fabric-selective	pr; brwn dol	1	64	−19.3	21.9	0.708397	1	2.9
Petroleum inclusions	dolomite wackestone (sequence I)	pr; brwn dol	1	59	−17.5	20.6			
		pr; brwn dol	1	<65, SP	N/A	N/A; low			
		pr; brwn dol	3	<65, SP	N/A	N/A; low			
		pr; brwn dol	2	<65, SP	N/A	N/A; low			
SM 30 m	Ooid grainstone (sequence I)	Not measured					0.708343	−6.2	2.1
SM 120.6 m	Fine-crystalline, fabric-selective	pr; dol	1	<65, SP	N/A	N/A; low	0.708233	3.1	3.2
Petroleum inclusions		pr; dol	2	<65, SP	N/A	N/A; low			
		pr; dol	7	<65, SP	N/A	N/A; low			
WRC 33.65 m	Medium-crystalline, partially fabric-	pr; brwn dol core	3	110–115	−9 to −8	11.7–12.9	0.709071	−3.4	2.8
	selective dolomite (sequence II)	pr; brwn dol core	5	105–115	−19.5 to −18.5	21.3–22.0			
		pr; brwn dol rim	5	105–115	−18 to −17	20.2–21.0			
		pr; brwn dol core	3	100–110	−5.3 to −5	7.9–8.3			
		pr?; brwn dol rim	4	105–115	−9.6 to −9.3	13.2–13.5			
		pr; brwn dol rim	3	80–90	−7.5 to −7.1	10.6–11.1			
		pr; brwn dol core	6	90–100	−7.1 to −6.8	10.2–10.6			
		pr; brwn dol rim	1	82	−9.9	13.8			
		pr; brwn dol core	5	80–85	−7.5 to −7.2	10.7–11.1			
WR 4 SIII	Medium-crystalline, non-fabric-	pr?; late, clear dol	2	100–110	−10.5 to −11.0	14.5–15.0	Not measured	−8.9	0.7
	selective dolomite (sequence III)	pr; late, clear dol	13	105–115	−19.0 to −20.0	21.7–22.4			
		pr; late, clear dol	3	100–110	−18.0 to −19.0	21.0–21.7			
		pr?; late, clear dol	6	105–110	−15.0 to −16.0	18.6–19.5			
		pr?; late, clear dol	4	100–110	−16.0 to −17.0	19.5–20.2			
		pr; late, clear dol	4	105–115	−15.0 to −16.0	18.6–19.5			
		pr; late, clear dol	5	90–100	6.3 to −6.7	9.6–10.1			
WR 4 SIII	Sparry calcite from a late-stage cemented fracture breccia	Unable to measure					0.715254	−20.2	−1.2
SH_J	Primary sparry calcite (sequence III)	pr?sec?; cc	2	<65, SP	N/A	N/A; low	Not measured	−4	0.9
		pr?sec?; cc	2	<65, SP	N/A	N/A; low			
		pr?; cc	5	45–55	−2.3 to −2.0	3.4–3.9			

SH_J	Medium-crystalline, non-fabric-selective dolomite over primary calcite (sequence III)	pr; brwn dol	1	89	−1.1	1.9	0.709029	−0.5	2.8
		pr; brwn dol	1	83	−0.8	1.4			
		pr; brwn dol	1	78	−0.7	1.2			
		pr; brwn dol	3	65–75	−0.6 to −0.3	0.5–1.1			
		pr; brwn dol	1	88	−1.3	2.2			
		pr; brwn dol	1	91	−0.8	1.4			
		pr; brwn dol	1	97	−1.1	1.9			
		pr; brwn dol	4	90–100	−3.4 to −3.1	5.1–5.6			
		pr; brwn dol	5	90–100	−3.3 to −2.8	4.7–5.4			
SM 2.95 m Petroleum inclusions	Sparry replacement calcite-filling brecciated vug (sequence I)	Unable to measure					0.708954	−16	1.2
WRBR_3a	Coarsely crystalline, fabric-destructive, and zoned dolomite from a late-stage calcite shattered breccia (sequence III)	pr?; brwn dol	1	113	N/A	N/A	0.709825	−5.1	2.8
		pr; brwn dol core	4	115–125	−10.5 to −10.0	13.9–14.5		−8.2	1.4
		sec?; brwn dol rim	5	130–140	>0; clath?	N/A		−4.8	3.1
		pr; brwn dol rim	1	138	−18.5	21.3		−7.2	3.3
		pr; brwn dol rim	4	125–130	−19.0 to −18.5	21.3–21.7		−3.2	4.5
		pr; brwn dol core	4	110–120	−10.6 to −10.2	14.2–14.6			
		pr; brwn dol core	2	130–140	−10.6 to −10.2	14.2–14.6			
		pr?; dol	4	95–105	−11.0 to −12.0	15.0–16.0			
		pr?; dol	4	100–110	−15.0 to −15.5	18.6–19.1			
		pr?; dol clast center	2	100–110	−9.5 to −10.0	13.4–13.9			
WRBR_3b	Sparry calcite from a late-stage calcite shattered breccia (sequence III)	pr?sec?; blky cc	1	125 (stretched?)	−5.5	8.6	0.727310	−17.2	9.2
		sec/psec; cc cmt	5	95–105	>0	N/A; low		−17.2	9.2
		sec/psec; cc cmt	2	100–110	>0	N/A; low		−18.0	4.6
		sec/psec; cc cmt	3	95–105	>0	N/A; low		−17.0	11.1
		sec/psec; cc cmt	5	100–110	>0	N/A; low		−17.5	11.5
		sec/psec; cc cmt	4	100–110	>0	N/A; low		−16.6	11.0
		sec/psec; cc cmt	4	95–105	>0	N/A; low			
		sec/psec; cc cmt	6	50–60	>0	N/A; low			
		sec/psec; cc cmt		highly variable	>0	N/A; low			
		sec/psec; cc cmt	8	55–65	>0	N/A; low			
WR 3.2	Sparry calcite from a late-stage calcite chaotic breccia (sequence III)	sec/psec; calcite cmt	1	61	>0	N/A; low	0.71599	−19.6	−1.0
		psec; calcite cmt	4	70–80	>0	N/A; low		−19.9	−0.8
		psec; calcite cmt	4	70–80	>0	N/A; low		−22.0	−1.6
		psec; calcite cmt	2	75–80	>0	N/A; low		−20.0	−0.8

Table 1. Continued

Sample**	Petrographic Description and Notes	Population***	Number of Inclusions Measured	$T_{h(aq)}$† (°C)	$T_{m(aq)}$†† (°C)	Salinity (wt.%)‡	Bulk Sample $^{87}Sr/^{86}Sr$	Inorganic Carbonate $\delta^{18}O$ (‰ PDB)	Inorganic Carbonate $\delta^{13}C$ (‰ PDB)
WR 3.2	Dolomite clast from a late-stage calcite-cemented chaotic breccia (sequence III)	pr?; dol clast edge	7	80–90	>0	N/A; low	Not measured	−3.5	0.7
		pr?; dol clast center	5	80–90	−7.7 to −8.1	11.3–11.8		−5.1	0.2
		pr; dol clast center	1	88	−7.9	11.6		−8.1	0.6
		pr; dol clast center	2	85–90	−7.8 to −7.9	11.5–11.6			
		pr; dol clast center	2	80–85	−8.1 to −8.2	11.8–11.9			
		pr; dol clast center	4	80–90	−19.5 to −20.5	22.0–22.7			
		pr; dol clast center	1	86	−18.5	21.3			
		pr; dol clast center	2	85–90	−18.5 to −19.0	21.3–21.7			
P 58	Sparry calcite from a late-stage calcite-cemented chaotic breccia	sec/psec; cc cmt	3	50–60	>0	N/A; low	Not measured	−18.5	−0.3
		sec/psec; cc cmt	3	55–65	>0	N/A; low		−21.5	−2.3
		sec/psec; cc cmt	1	62	>0	N/A; low		−17.9	0.1
		sec/psec; cc cmt	2	55–65	>0	N/A; low		−21.3	−1.9
		sec/psec; cc cmt	2	55–65	>0	N/A; low			
		sec/psec; cc cmt	1	59	>0	N/A; low			
		sec/psec; cc cmt	1	55	>0	N/A; low			
P 58	Dolomite clast from a shattered breccia	pr?; dol clast edge	1	97	>0	N/A; low	Not measured	−7.4	1.3
		pr?; dol clast edge	1	99	>0	N/A; low		−7.6	1.2
SM 4 m Petroleum Inclusion	Sparry calcite from a late-stage calcite-cemented fracture (sequence I)	pr/sec; cc cmt	2	100–110	>0	N/A; low	0.708948	−19.8	−5.7
		pr/sec; cc cmt		Stretched	>0	N/A; low		−21.3	−7.8
		pr/sec; cc cmt		Stretched	>0	N/A; low		−19.3	−6.6
SM 4 m	Fine-crystalline, fabric-selective dolomite wall rock (sequence I)	pr; dol	3	100–110	>0	N/A; low	Not measured	−4.4	3.2
		pr; dol	1	92	−2.8	4.7			
		pr; dol	1	88	−4.8	7.6			
		pr; dol	3	85–95	N/A	N/A; low			
SM 1.95 m Petroleum Inclusion	Late-stage calcite-cemented fracture (sequence I)	pr?; cc zone 1	4	130–140	>0	N/A; low	0.709664	−22.7	−7.2
		pr?; cc zone 3	6	120–130	>0	N/A; low			
		pr?; cc zone 3	4	120–130	>0	N/A; low			
		pr?; cc zone 3	5	130–140	>0	N/A; low			
		pr?; cc zone 3	8	130–140	>0	N/A; low			
		sec?; cc zone 3	2	120–130	>0	N/A; low			
		sec?; cc zone 3	4	120–130	>0	N/A; low			
		sec?; cc zone 3	3	120–130	>0	N/A; low			
		pr?; cc zone 3	3	130–140	>0	N/A; low			

SH_G	Late-stage calcite-cemented fracture (sequence III)	Not measured	0.712385	−22.1	−1.4
SH 76–77 m	Late-stage calcite-cemented fracture (sequence I)	Not measured	0.711731	−21.7	−0.7
SH 103 m	Late-stage calcite-cemented fracture (sequence II)	Not measured	0.712129	−22.8	0.4
SH 81.1 m	Late-stage calcite-cemented brecciated vug (sequence II)	Not measured	0.711486	−21.8	−0.9

*A primary fluid-inclusion population is the number of inclusions sampled from a single-cystal growth zone.
**Samples are from the following locations: SM = Sheep Mountain anticline; SH = Shoshone Canyon; WRBR = Wind River Boysen reservoir; and P and WRC = Wind River Canyon.
***pr = primary inclusion; dol = dolomite; cc = calcite; cmt = cement; sec = secondary inclusion; psec = pseudosecondary inclusion.
†$T_{h(aq)}$ = homogenization temperature of aqueous inclusions. SP (single-phase inclusions) do not respond to tests, probable $T_h < 65°C$. Stretched = inclusion shape is highly irregular, suggesting the volume was stretched resulting in elevated $T_{h(aq)}$ and lower salinity values.
††$T_{m(aq)}$ = final melting temperature for aqueous inclusions. N/A = could not be determined.
‡Salinity is computed from the NaCl system. $T_{m(aq)} > 0$ and salinity = N/A low denotes metastable ice melting representative of salinities <5 wt.% NaCl (D. Hall, 2005, personal communication).

Marine Phreatic Environment: Dolomite and Calcite

Modern marine calcites ($\delta^{18}O$ = 0–2‰) are in equilibrium with marine fluids ($\delta^{18}O$ = 0‰ standard mean ocean water [SMOW]) at standard surface seawater temperature (approximately 25°C). Mississippian marine carbonate values from Veizer et al. (1999) ($\delta^{18}O$ = −4.8 to −3‰) and this study ($\delta^{18}O$ = −2.25–5‰) are more depleted. Sample SH_J ($\delta^{18}O$ = −4‰) (Figure 14) is an example of a preserved Mississippian marine calcite that precipitated from normal-marine waters. Hypersaline carbonates include SM 120.6 m (395.6 ft) and SM 8.15 m (26.7 ft); these samples are fine-crystalline dolomites from restricted lagoonal facies and have low-temperature homogenization values, hypersaline values, and enriched $\delta^{18}O$ values, suggesting that they precipitated in a restricted and evaporitic marine environment (Craig et al., 1963; Lloyd, 1964). These samples may also have been partially reset isotopically during leaching of low Mg-calcite allochems and successive burial dolomitization. Nonradiogenic Sr isotope values and enriched $\delta^{18}O$ values suggest that little to no resetting of these samples has occurred during deep-burial diagenesis. The presence of single-phase fluid-inclusion populations also suggests that these samples (SM 120.6 m [395.6 ft] and SM 8.15 m [26.7 ft]) are well preserved and derived from the low-temperature phreatic zone. Low- to elevated-temperature petroleum inclusions from the dolomites at Sheep Mountain, samples at 120.6 m (395.6 ft) and 8.15 m (26.7 ft), suggest that the Madison Formation was charged by hydrocarbons during pre-Laramide burial diagenesis (Figure 16).

Burial Phreatic Environment: Geothermal Dolomite

The 65–115°C range of homogenization temperatures from dolomites, SH_J, and WRC 33.65 m (110.4 ft) is consistent with temperatures generated by standard thermal gradients of 25–30°C/km at depths near 3–4 km (1.8–2.5 mi) (Peterson 1986; Choquette and James, 1987; Machel and Lonne, 2002). Salinities from these samples indicate that they recrystallized from a mixture of hypersaline fluids and fluids with salinities less than seawater concentrations. Our geochemical data indicate the presence of multiple fluids affecting these rocks during burial diagenesis. For example, replacive dolomite fabric at Shoshone Canyon has low salinities (fluid salinities range from 0.5 to 5.4 wt.% NaCl and are dominantly within the 1–2% range), suggesting that Shoshone Canyon dolomites may have

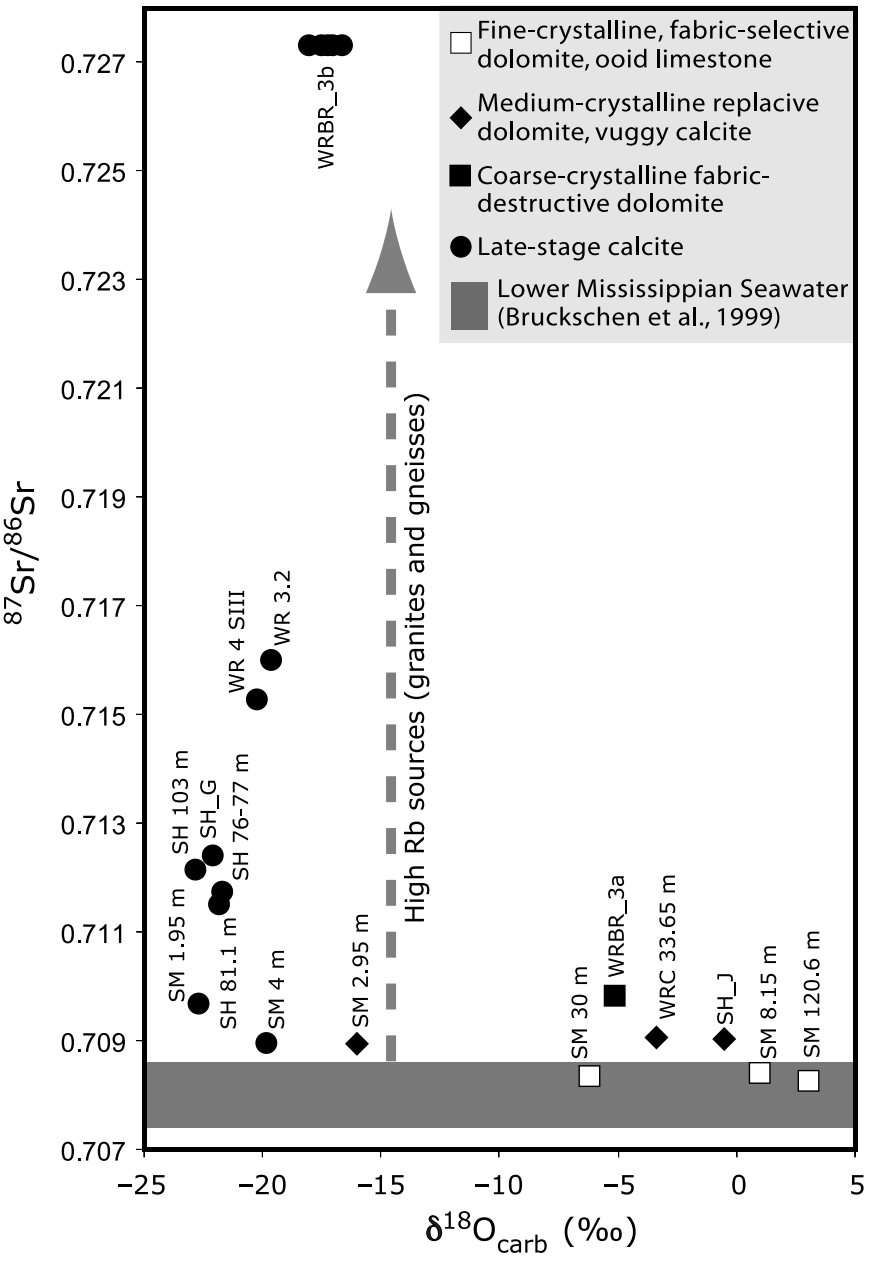

Figure 13. Strontium and oxygen isotope crossplot showing different types of carbonate rock occurring throughout the Owl Creek thrust sheet, Madison Formation. See Table 1 for sample descriptions. Fine-crystalline dolomites (SM 120.6 m [395.6 ft] and SM 8.15 m [26.73 ft]) and an oolitic limestone (SM 30 m [98 ft]) have Sr values that are within the range for Mississippian seawater as defined by Bruckschen et al. (1999). Medium-crystalline, replacive dolomites (SH_J and WRC 33.65 m [110.40 ft]) and vuggy calcites (SM 2.95 m [9.67 ft]) have Sr values that are intermediate to Mississippian seawater samples and late-stage calcite. Coarsely crystalline, fabric-destructive dolomite (WRBR_3a) from the tip of the Owl Creek thrust sheet has more radiogenic values than diagenetic vuggy calcite and medium-crystalline dolomites. Late-stage calcites have the most radiogenic Sr isotope ratios and most depleted oxygen isotope values. See Table 1 for sample descriptions.

experienced minor amounts of mixing zone dolomitization during early burial diagenesis. In contrast, inclusions from the rims of medium-crystalline and partially fabric-selective dolomite samples from Wind River Canyon indicate that later burial diagenesis was dominated by hypersaline fluids, with salinities ranging from 8.0 to 22.0 wt.% NaCl. Possible sources for such high salinities come from Mississippian, Pennsylvanian, and Permian evaporites (Hanshaw et al., 1978). Interestingly, there has been little or no resetting of their isotopic values ($\delta^{13}C = 2.8‰$, $\delta^{18}O = -3.4$ to $-0.5‰$) as compared to Mississippian seawater values reported by Veizer et al. (1999), suggesting that diagenesis was dominated by a rock-buffered system. These dolomites are also slightly radiogenic, which suggests that fluid-migration pathways may have interacted with radiogenic rocks such as the underlying clastic sedimentary strata and/or Precambrian basement.

Burial Phreatic Environment: Hydrothermal Dolomite

Sample WRBR_3a is coarsely crystalline and interpreted to be a fabric-destructive geothermal to hydrothermal (Figure 14) dolomite. This sample contains a

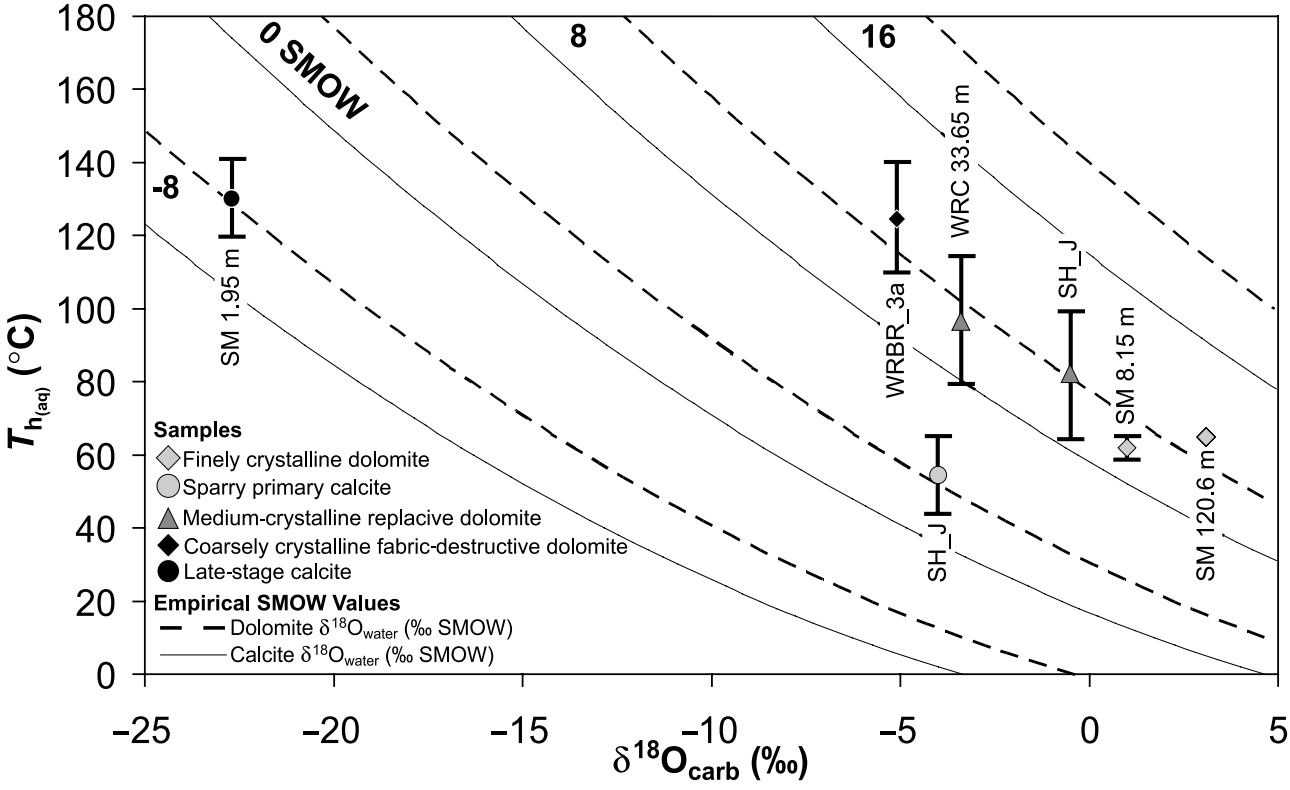

Figure 14. Crossplot of oxygen isotopes versus homogenization temperature of aqueous inclusions. All data derive from primary inclusion populations. The data have been superimposed over empirically derived dolomite and calcite standard mean ocean water (SMOW) values (Epstein and Mayeda, 1953). Enrichment in SMOW values correspond to increasing salinities. Zero SMOW corresponds to seawater at standard near-surface conditions. The hottest entrapment temperatures are from the late-stage calcite (120–140°C) and shattered dolomite breccia (110–140°C). Sample descriptions are in Table 1.

bimodal distribution of hypersaline values and homogenization temperatures, indicating that the dolomite formed over a temperature range and during progressive heating to temperatures hotter than those generated by standard burial conditions. Lower salinities and homogenization temperatures occur in the cores with higher salinities and homogenization temperatures occurring in the rims. Therefore, we interpret that the cores of this dolomite formed under geothermal conditions, whereas the outer rim is considered hydrothermal in origin. Sources for the hypersaline values in the rim of the dolomite may have been derived from Mississippian, Pennsylvanian, and Permian evaporites (Hanshaw et al., 1978). This sample also has minor amounts of secondary quartz, a hydrothermal mineral, as well as Sr isotope ratios that are more radiogenic (Figure 13) than the geothermal dolomite. In our study area, hydrothermal dolomite only occurs at the isostatically collapsed, leading edge of the Owl Creek thrust sheet (Figure 3B).

Surficial Karst and the Anhydrite Solution Collapse Breccias

Stable oxygen isotope values of the other types of breccias (−12.7 to +0.9‰) affecting the Madison Formation are considerably more enriched than the $\delta^{18}O$ values found in the tectonic-hydrothermal late-stage calcite (−26.5 to −15.1‰). The difference in $\delta^{18}O$ values between the two types of breccias indicates that the late-stage calcite derives from a significantly more depleted fluid than the other two breccias. Relatively more depleted values in the late-stage calcite also suggest that they precipitated at higher temperatures than the other breccias.

Burial Phreatic Environment: Tectonic-Hydrothermal Late-Stage Calcite

The large range in depleted $\delta^{18}O$ and $\delta^{13}C$ values, the wide range in radiogenic Sr isotope ratios, and the presence of metastable inclusions with the hottest

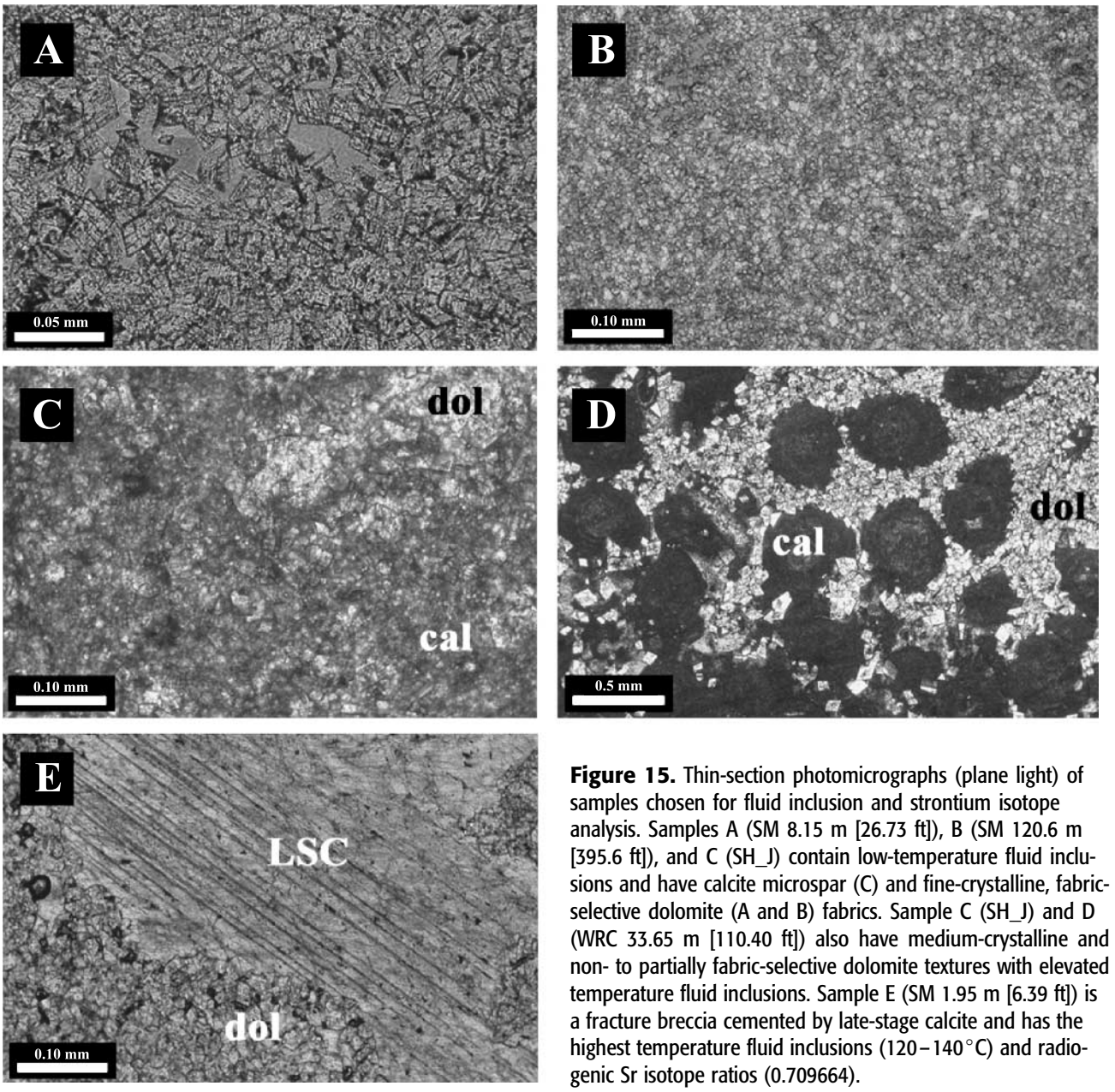

Figure 15. Thin-section photomicrographs (plane light) of samples chosen for fluid inclusion and strontium isotope analysis. Samples A (SM 8.15 m [26.73 ft]), B (SM 120.6 m [395.6 ft]), and C (SH_J) contain low-temperature fluid inclusions and have calcite microspar (C) and fine-crystalline, fabric-selective dolomite (A and B) fabrics. Sample C (SH_J) and D (WRC 33.65 m [110.40 ft]) also have medium-crystalline and non- to partially fabric-selective dolomite textures with elevated temperature fluid inclusions. Sample E (SM 1.95 m [6.39 ft]) is a fracture breccia cemented by late-stage calcite and has the highest temperature fluid inclusions (120–140°C) and radiogenic Sr isotope ratios (0.709664).

temperatures suggest that the fluid responsible for precipitating the late-stage calcite is derived from mixed meteoric Laramide recharge and subsurface hydrothermal brines. These results also suggest that the calcite precipitated in a water-dominated or open diagenetic system, whereas the geothermal dolomites have a narrow range in $\delta^{18}O$ and $\delta^{13}C$ values and a narrow range in $^{87}Sr/^{86}Sr$ ratios, implying a recrystallization under a rock-buffered or relatively closed diagenetic system at thermal equilibrium with standard geothermal gradients. If the late-stage calcite fluids were derived strictly from a meteoric source, one would expect to find a smaller range in $\delta^{18}O$ and $\delta^{13}C$ values as well as more enriched $\delta^{18}O$ values similar to those from the speleothem deposits at Baldy Mountain, Montana (Figure 10).

Using the average $\delta^{18}O$ value (-17 ‰) of the Baldy speleothem (Figure 10) as the proxy for Laramide-age meteoric calcite in equilibrium with groundwaters having $\delta^{18}O$ values ranging from about -19 to -18 ‰ SMOW would yield a calcite in equilibrium with meteoric groundwater between 12.3 and 8.5°C (temperature equation from Epstein and Mayeda, 1953). These water values are also within the range of those

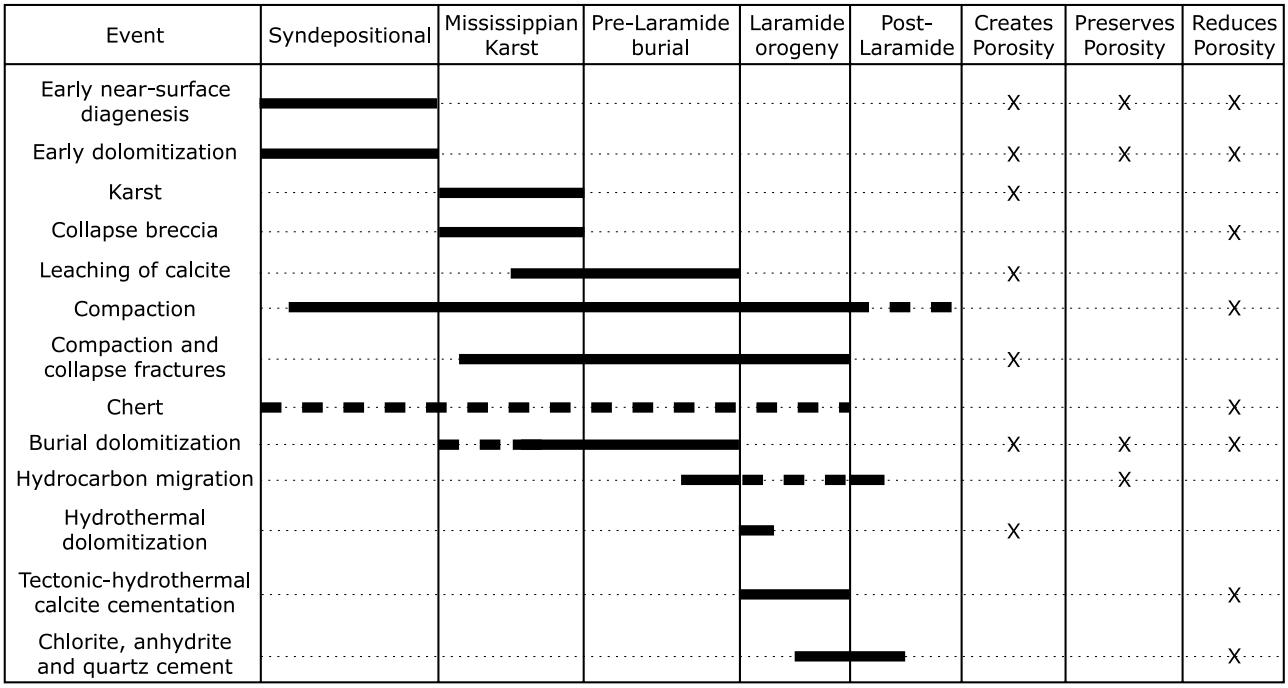

Figure 16. Paragenetic sequence and timing of each event that affected the Madison Formation and porosity development (modified from Smith et al., 2004). Data for this chart are derived from subsurface and outcrop locations of the Wind River and Bighorn basins.

measured from modern meteoric groundwater (−24 to −2 ‰ SMOW) located in the Turkey Creek Basin, Colorado Front Range (Humphrey et al., 2005). If Laramide-age meteoric groundwater was the sole source for precipitating the late-stage calcite at a temperature range between 120 and 140°C, the calcite would have $\delta^{18}O$ values from −47.6 to −42.0 ‰, assuming there is a 1 ‰ fractionation per 4.3°C change in temperature (Epstein and Mayeda, 1953; Epstein et al., 1953). The empirically derived data are significantly more depleted in ^{18}O than the measured values ($\delta^{18}O$ = −26.5 to −15.1 ‰); Madison late-stage calcite is in equilibrium with fluids having $\delta^{18}O$ values = −10.5–3 ‰ SMOW, which include the range from freshwater to hypersaline values. Either the understaturated meteoric groundwaters incorporated enriched $\delta^{18}O$ from the dissolution of the overlying carbonates during migration into the subsurface, and/or the meteoric waters eventually mixed with hot subsurface brines having enriched isotopic compositions of a relatively more rock-buffered system. Considering that metastable inclusions found in the late-stage calcite are most common of inclusions with salinities less than 5 wt.% NaCl and that the host or wall rock contains hypersaline inclusions (~22 wt.% NaCl) and relatively enriched $\delta^{18}O$ values (−13 to 5 ‰) that are interpreted to have formed in equilibrium with the burial and marine waters, the late-stage calcite-bearing fluids likely precipitated from an intermediate mixture of downward percolating meteoric waters and hot subsurface brines.

The late-stage calcite shows a wide range in $\delta^{18}O$ values (−26.5 to −15 ‰), indicating that the tectonic-hydrothermal fractures and breccias did not all form simultaneously and from a single temperature fluid (Figure 11). Microdrilling results from individual samples, however, show that there is very little variability in $\delta^{18}O$ values across an individual calcite cement vein, suggesting that it precipitated from a very similar fluid possibly during one tectonic event (Figure 12). Thus, we conclude that cementation occurred rapidly, thereby preventing significant isotopic exchange and temperature change with the fluid and surrounding host rock. The variability in the $\delta^{18}O$ values might be explained by episodic earthquakes during Laramide deformation. Each of these events was responsible for forcefully injecting late-stage calcium and carbonate-bearing fluid into the Madison Formation with slightly variable hydrothermal temperatures, variable $\delta^{18}O$ values, and low variant $\delta^{13}C$ values in an outcrop. We observed a regional trend in the $\delta^{18}O$ values showing that samples from the isostatically collapsed zone at Wind River Canyon (Figure 11) have the most enriched

$\delta^{18}O$ values, whereas samples located farther to the north of the frontal part of the Owl Creek thrust have the most depleted $\delta^{18}O$ values (Figure 11) for the Wind River Canyon. Samples from Sheep Mountain have similar $\delta^{18}O$ values to the Wind River Canyon, and the range from both locations is intermediate to the range reported from the Shoshone Canyon (Figure 11), which contains the most depleted $\delta^{18}O$ values in the Madison Formation. The range in $\delta^{18}O$ values reported across the Bighorn Basin might be explained by varying fluid temperature during brecciation episodes, where the hottest fluids are in equilibrium with the most depleted $\delta^{18}O$ values. This would suggest that late-stage calcites from the Shoshone Canyon precipitated from the hottest hydrothermal fluids.

Little variability in $\delta^{13}C$ values is present in each outcrop, but a large variability exists from outcrop to outcrop (Figure 11). This variability might be attributed to the structural setting and carbon source (Figure 3). For example, Boysen reservoir samples are from the shattered breccia at the leading edge of the Owl Creek thrust sheet and have the most enriched $\delta^{13}C$ values ($\sim$12‰) measured in this study (Figure 11). These carbon isotope values are abnormally high for most carbonates (Deuser, 1970; Hudson, 1977). Although the usual explanation is that elevated $\delta^{13}C$ values arise from the process of methanogenesis (Irwin et al., 1977), this origin is incompatible with the high-temperature association. An alternative explanation is that the elevated $\delta^{13}C$ values arise as a result of equilibrium exchange between CH_4 and CO_2 at elevated temperatures more than 100°C (Murata et al., 1969). Isotopic exchanges between CH_4 and CO_2 are known to take periods in excess of 10^9 yr at sedimentary temperatures, but can proceed relatively fast at temperatures higher than 100°C. Assuming that the source of the methane is the thermogenic cracking of bitumen ($\delta^{13}C_{org} \approx -27$‰) found filling vuggy porosity at Shoshone Canyon, then the $\delta^{13}C_{carb}$ should be several per mil more negative (~ -30‰). At temperatures of about 200°C, there is minimal fractionation in C between CO_2 and calcite, and therefore, one can simply estimate the ΔCH_4-CO_2 as the difference between the most isotopically enriched carbonates and the presumed isotopic composition of the methane (ΔCH_4-$CO_2 \approx 40$‰; Bottinga, 1969). This is consistent with equilibrium between CH_4 and CO_2 at a temperature of 180°C and is therefore in agreement with data obtained from fluid inclusions and oxygen isotopic data.

The presence of elevated temperature petroleum inclusions in all hydrothermal late-stage calcite fluid inclusion ($T_{h(aq)}$ = 120–140°C) samples from Sheep Mountain (Table 1) suggests that the oxygenation of organic carbon and the generation of an isotopically light CO_2 source is responsible for the relatively depleted $\delta^{13}C$ values in the carbonate (Figure 11) (Donovan, 1974). Samples from the Wind River Canyon and Shoshone Canyon have the smallest range in $\delta^{13}C$ values (Figure 11) and are intermediate to Sheep Mountain and Wind River Canyon and Boysen reservoir samples. Wind River Canyon and Shoshone Canyon samples are interpreted to be in equilibrium with CO_2 produced from the dissolution of the surrounding carbonate by freshwater that mixed with heated brines in the subsurface.

Petroleum inclusions occur in the fine-crystalline, fabric-selective dolomites from sequences I and IIa and also in the late-stage calcite at Sheep Mountain anticline. The presence of dual petroleum inclusions indicate that the Madison Formation was charged with hydrocarbons once during pre-Laramide dolomite formation and again during the tectonic-hydrothermal activity of the Laramide orogeny (Figure 16). The timing of the second migration corroborates results from Smith et al. (2004), who also provide evidence that hydrocarbon migration occurred toward the end of the Laramide orogeny.

All outcrop locations are structurally similar in that they are located near major high-angle basement-cored faults (Figure 3). These faults are interpreted to be the conduits for vertical migration of the fluids from basement rock to the Madison Formation during episodes of tectonic activity. The chemical signature of the late-stage calcite provides strong evidence that it precipitated from these fluids. The strontium isotope values of the late-stage calcite are between 0.7089 and 0.7273 and document the incorporation of strontium from basement rocks like the pink granites (0.726) of the Beartooth Mountains, Montana (Lafrenz et al., 1986), the continental crust (0.7155–0.7165; Burke et al., 1982), feldspathic basement (0.7195; Tucker and Wright, 1990), Precambrian gneisses (0.712–0.726; Faure et al., 1963), and/or old shields (feldspathic crust) (0.712–0.730; Holland 1984).

The Sr isotope ratios display a wide range of values (Figure 13), but are distinct for each location, which might be related to the structural setting and the amount of basement displacement or deformation at each location. Strontium isotope ratios are highest at the Wind River Canyon and Boysen reservoir and decrease progressively from the Wind River Canyon, Shoshone Canyon, to Sheep Mountain anticline. One interpretation is that the fluids remained in contact with the

basement for variable periods, or it interacted with larger volumes of Rb-rich basement and incorporated more of the radiogenic ^{87}Sr than settings with less basement displacement or deformation. For example, the most radiogenic values are derived from the isostatically collapsed zone at the tip of the southern Owl Creek thrust fault (Figures 3B, 13), which accommodates nearly 16 km (10 mi) of basement overhang and more than 9000 m (30,000 ft) of structural relief (Gries, 1983; Paylor and Lang, 1990). This frontal thrust is displacing basement rocks and extends far into the radiogenic basement. Thus, the Sr content in the fluids migrating along the Boysen and Owl Creek master fault system would be expected to be enriched by the radiogenic Precambrian basement rocks. The measured section at the Wind River Canyon has the second most radiogenic ratios. It is located to the north of the Boysen reservoir and away from fluid-migration pathways in the isostatically collapsed zone of the frontal thrust, but obviously still received waters enriched from the basement.

The Shoshone Canyon measured section is located in the southwestern limb of the Rattlesnake Mountain anticline, which accommodates approximately 6000 m (20,000 ft) of structural relief on the basement surface and less than 1 mi (1.6 km) of basement overhang (Figure 3A) (Erslev, 1990). Late-stage calcite-bearing fluids would have interacted with smaller volumes of basement than those from the frontal thrust. Its Sr ratio is indeed lower, and some of the values are similar to those from the Wind River Canyon. The Sheep Mountain late-stage calcites have the lowest Sr ratios. The interpreted thrust fault below the Sheep Mountain measured section does not penetrate the Madison Formation and is accommodated by a series of fracture and joint sets in the anticline (Bellahsen et al., 2004). This is an immature thrust fold with the least basement displacement (Figure 3C), which suggests that subsurface fluids may have mixed the least with radiogenic basement.

TECTONIC BRECCIATION AND HYDROTHERMAL LATE-STAGE CALCITE CEMENTATION

Hydrothermal activity develops within seismically active compressional regimes, where crustal thickening or thrust stacking can lead to progressive dewatering and maintenance of suprahydrostatic pressure gradients in the fluid (Sibson, 1990). Transtensional or extensional faults are also regions that accommodate upwelling of hydrothermal fluids along subvertical hydrofractures (Sibson, 1990). The precipitation of hydrothermal cements is controlled by two factors that focus the hydraulic fracturing and precipitation in the uppermost 2000–500 m (6560–1640 ft) (Figure 17A) (Henley, 1985). First, boiling is induced and maintained within geothermal systems only at these depths, and second, fluids under hydrostatic pressures at these depths may form clusters of vertical fractures by hydraulic fracturing. Drummond and Ohmoto (1985) and Henley (1985) show that rapid hydrothermal cementation can be achieved by rapid pressure drops during earthquake rupturing, which induces fluid flashing or boiling. Rupturing during earthquake activity acts like a fault valve, which causes CO_2 effervescence during large pressure changes (Robert and Kelly, 1987; Morse and Mackenzie, 1990). Large pressure fluctuations are commonly followed by rapid hydrothermal cementation as evidenced by wall rock breccias and dilational fractures supported by matrix cement (Sibson, 1985).

The structural settings of the study area are prone to tectonic-hydrothermal activity as documented by Drummond and Ohmoto (1985), Henley (1985), and Sibson (1990). Furthermore, hot spring activity at Thermopolis in the northern entrance to the Wind River Canyon documents that circulation of hot subsurface fluids and calcite cementation is still occurring and might have been active in the Bighorn Basin since the Laramide orogeny. Tufa deposits are also present in the Shoshone Canyon and overprint part of the sedimentary section below the measured Madison section, indicating active groundwater circulation of calcite-saturated fluids.

The morphology, distribution, and geochemistry of the late-stage, calcite-cemented fractures and breccias suggest that brecciation of the rock was episodic and caused by the explosive injection of hot fluids in the strata from which the late-stage calcite precipitated quickly after the brecciation event. Figure 17 illustrates the conceptual model for these processes based on our data. The most intense brecciation occurred at the leading edge of the Owl Creek thrust sheet at Boysen State Park. A spatial trend and an increase of chaotic and shattered breccias toward the front of the thrust sheet exist (Figure 3B). We envisage the waters involved with the brecciation and cementation to be undersaturated meteoric groundwaters, which migrated into the burial environment while dissolving and incorporating Ca^{2+} and CO_3^{2-} from the dissolution of the surrounding carbonates (Figure 17A). In the burial environment, these fluids were heated and mixed with hypersaline

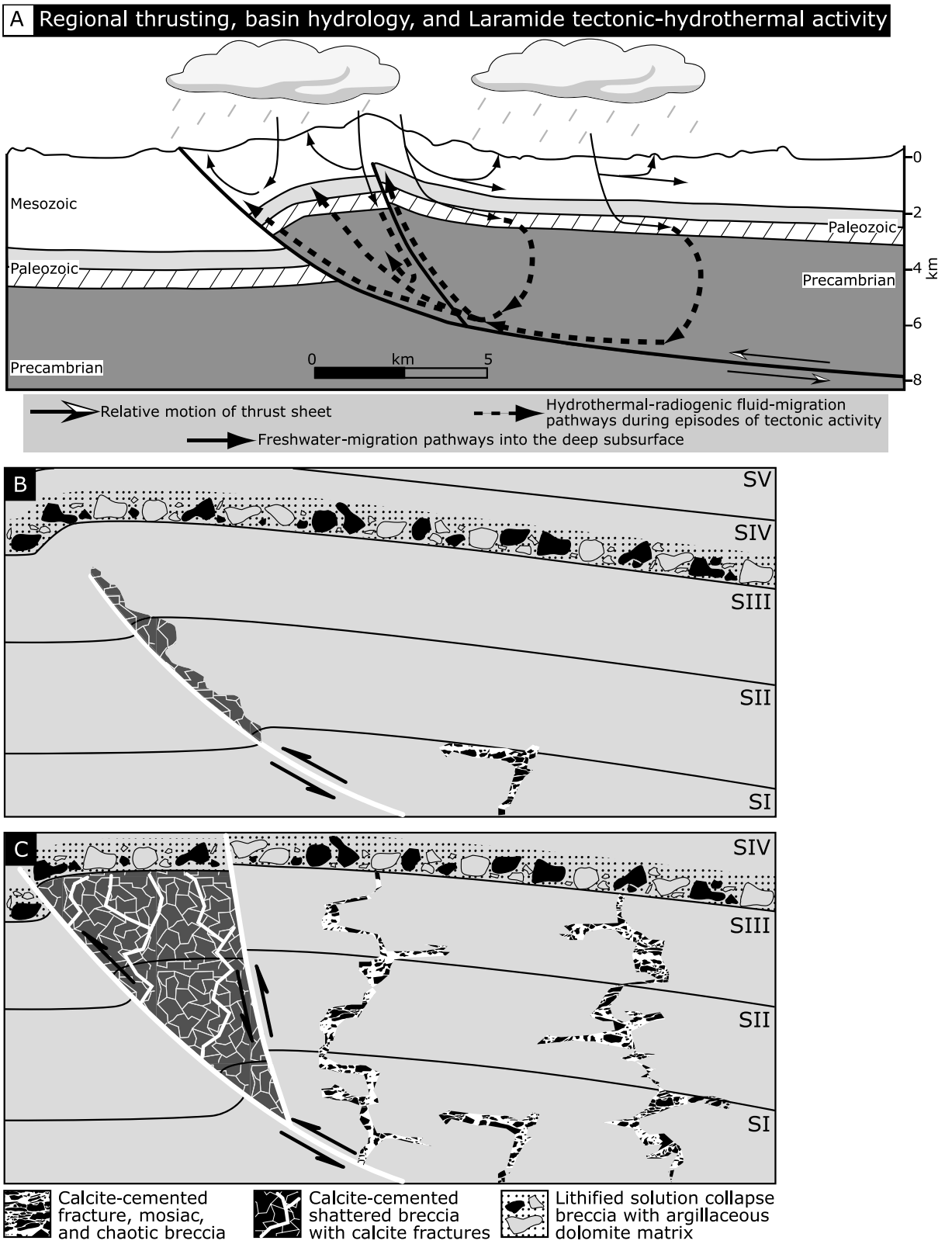

Figure 17. Hydrothermal activity resulting in brecciation and fracturing is sourced by downward-percolating waters that mix with radiogenic basement (A). The hot waters are expelled and cycled along basement-rooted thrusts into the overlying strata. The injection (B and C) of the hot fluids is similar to dike formation as it cuts into the strata in an irregular and unpredictable subvertical pattern. The brecciation is most intense at the front of the thrust sheet, where it produces a shattered breccia. Away from the frontal thrust, the amount of brecciation varies and produces the fracture, mosaic, and chaotic breccias. The width of B and C is approximately 5 km (3.1 mi).

brines in contact with deeply buried parts of radiogenic basement rock. Compressional forces during the Laramide orogeny and episodes of Laramide tectonic activity forced the migration of fluids along basement-cored thrust faults and as overpressured injections into the overlying Madison Formation. The expulsion of the waters away from the master faults during earthquake events resulted in hydrobrecciation and hydrofracturing of the host rock (Figure 17B, C). The calcite cements in the breccia are interpreted to have precipitated rapidly during pressure release in response to earthquake-induced rupturing and brecciation of the host rock. Robert and Kelly (1987) and Morse and Mackenzie (1990) show that the fluid response to rupturing of the host rock can cause large pressure fluctuations and phase separation of CO_2 from the fluid, followed by rapid hydrothermal cementation (Sibson, 1985). The rupturing event was rapid and explosive in nature based on the intense deformation styles documented in the Madison breccias and fractures.

The regional distribution of the tectonic-hydrothermal fractures and breccias has implications for understanding lateral variability of structurally controlled hydrologic systems across Laramide basins and spatial variability in the geochemistry of pore fluids from the center of these basins extending to their margins. Although the preservation between outcrop and subsurface locations in the Madison Formation is remarkably similar with respect to pre-Laramide diagenetic textures such as porosity, permeability, and rock fabric (Crockett, 1994; Moore, 1995, 2001), the diagenetic manifestations resulting from the Laramide tectonic-hydrothermal activity are significantly different. For example, breccias and fractures from the Elk Basin in the Bighorn Basin (Elk Basin Madison 122 and Northwest Elk Basin Madison 8; Sonnenfeld, 1996b) are cemented by late dolomite and massive amounts of late anhydrite and show an absence of tectonic-hydrothermal late-stage calcite cements. Sonnenfeld (1996b) also shows a southeast to northwest trend of increasing amounts of anhydrite-plugged macroporosity in the central and northern Bighorn Basin. This suggests that meteoric waters for the Tensleep aquifer (Doremus, 1986; Jarvis, 1986; Spencer, 1986) and the Madison and Bighorn dolomite aquifer (Sonnenfeld, 1996b) may have interacted less with deeply buried parts of the basin center than the basin margins. Such a scenario could explain the late dolomite and anhydrite plugging documented at depth in the Bighorn Basin. Alternatively, the Elk Basin was simply too far away from the main thrusts to be intruded by overpressured waters.

In contrast, a core from the Wind River Basin (Beaver Creek field 137, located just south of the southern Owl Creek Mountains) has two late-stage calcite cemented fractures ($\delta^{13}C = -0.4‰, -0.2‰$ and $\delta^{18}O = -12.8‰, -14.3‰$) and one fracture breccia ($\delta^{13}C = 0.1‰$ and $\delta^{18}O = -12.5‰$) at approximately 3628 to 3648 m (11,902 to 11,968 ft). These values are more enriched than the late-stage calcite measured from Bighorn Basin outcrops ($\delta^{18}O = -26.5$ to $-15.1‰$). The isotopic variability from basin to basin suggests that the fluids in the subsurface of the Wind River Basin may have been derived from a relatively more ^{18}O-enriched and possibly more hypersaline fluid than the fluids that dominated the margins of the Bighorn Basin during the Cretaceous. Variable chemistry from the late-stage calcites across the two basins supports the notion presented by Huntoon (1993) and Sonnenfeld (1996b), that the Laramide uplift structures, such as the homoclinal margin of the southern Bighorn Basin, favor strong basin-directed recharge, and that the fault-severed margin of the northern Wind River Basin favors limited basin recharge. Fluids precipitating late-stage calcite in the fault-severed northern margin of the Wind River Basin may have longer residence times in the sedimentary rock column and would be more enriched in ^{18}O than those from the homoclinal southern margin of the Bighorn Basin.

Implications of Tectonic-Hydrothermal Calcite Cementation for Reservoir-Quality Carbonates

Tectonic-hydrothermal late-stage calcite cementation ultimately reduces the porosity and permeability of reservoir quality in the carbonates of the Madison Formation. Madison outcrops, the Madden gas field, and Beaver Creek core 137 document good porosity (intercrystalline and vuggy) and permeability for samples unaffected by late-stage calcite cementation (Figure 18A–C). In contrast, samples with late-stage calcite have poor porosity and permeability because fracture, intercrystalline, and vuggy porosity is occluded by calcite (Figure 18D–F) (Westphal et al., 2004). In the Bighorn Basin, porosity and permeability in outcrop and subsurface are very similar in the Madison Formation (Moore, 2001; Smith et al., 2004; Westphal et al., 2004). Porosity and permeability, and thus, reservoir quality, is mostly dependent on the original sedimentary texture that affects crystal size of the subsequent dolomites. Best-fit lines between porosity and permeability for different textures show that the exponent increases from mudstones to wackestones to packstones to grainstones

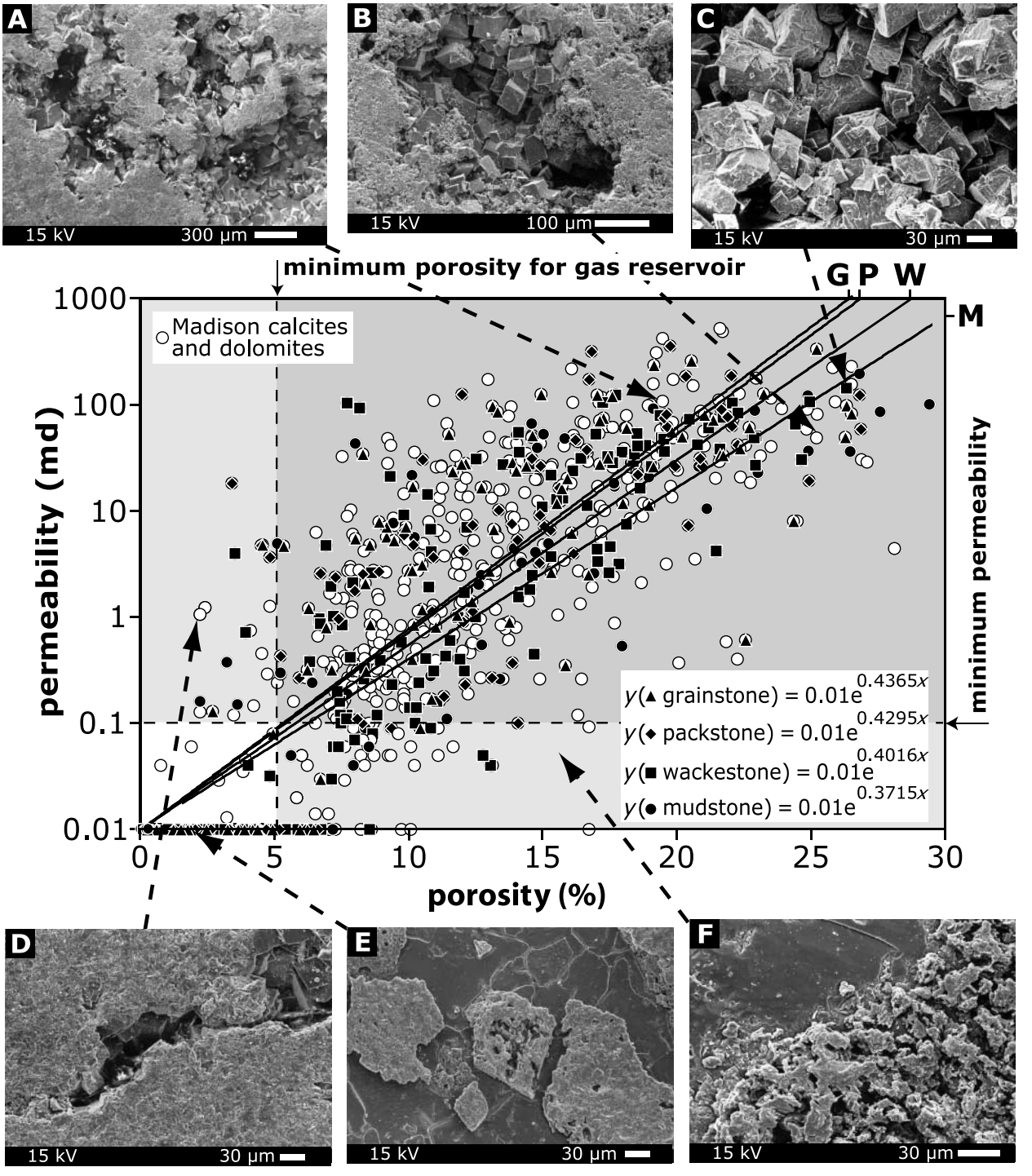

Figure 18. Porosity and permeability crossplot with scanning electron photomicrographs of fine- to medium-crystalline dolomites from the Madison Formation. The permeability and porosity distribution has a wide scatter, which ranges from high to low reservoir-quality values. Upon closer examination, dolomite samples that are grouped according to texture yield different trend lines; the exponential best fit shows that the exponent increases from mudstones to wackestones to packstones to grainstones. The most significant control over permeability and porosity is cementation by late-stage calcite. Samples A–C are of reservoir-quality dolomite unaffected by late-stage calcite cementation. Samples A and B show interconnected vuggy porosity, and sample C has preserved intercrystalline porosity. Samples D–F show porosity and permeability reduction by late-stage calcite cementation of fracture, intercrystalline, and vuggy porosity, respectively. Open circles are calcite and dolomite samples taken throughout the Madison Formation, Wyoming and Montana (Smith et al., 2004; Westphal et al., 2004). Dolomite mudstones are represented by black circles, dolomite wackestones by black squares, dolomite packstones by black diamonds, and dolomite grainstones by black triangles.

(Smith et al., 2004). Westphal et al. (2004) showed that dolomite grainstones have larger crystal sizes than packstones, and packstones have larger crystal sizes than wackestones, which are larger than mudstones (Lucia, 1995). As a result, grainstones have higher permeability than packstones, packstones have higher permeability than wackestones, and wackestones have higher permeability than mudstones, all with equal porosity. The $\delta^{18}O$ values of the fine-crystalline stratiform mudstone and wackestone dolomites are enriched up to +5‰ (Figure 10), which indicates dolomitization in an evaporative marine environment (Craig et al., 1963; Lloyd, 1964). Petrographic evidence shows that initial dolomite was in the form of poorly ordered dolomites that experienced later recrystallization and stabilization in the burial environment (Smith, 1991; Smith and Dorobek, 1993). During the Laramide tectonic-hydrothermal activity, these porous, reservoir-quality dolomites are dissected by healed fractures and breccias, which act to compartmentalize horizontal flow units and decrease reservoir quality (Westphal et al., 2004).

In the Wind River area, Lysite Mountain, and Buffalo Creek area, tectonic-hydrothermal breccias occur preferentially in the mudstones to wackestones of sequence III, in the form of large, vertical, calcite-healed breccia corridors (Westphal et al., 2004). In the Shoshone and Sheep Mountain sections, breccias and healed fractures occur preferentially in sequences I and II, but again predominantly in the mud and wackestone intervals (Figure 2). The breccias and fractures appear to terminate at or near the well-lithified sequence IV anhydrite solution collapse breccia (Figure 17C). Sequences I–III are either completely or partially dolomitized, whereas sequence IV is predominantly limestone with low (0–10%) porosities (Smith et al., 2004; Westphal et al., 2004). In the deeply buried reservoirs of the Bighorn Basin, these limestones are essentially the top seal. Less important vertical flow barriers are the well-cemented, low-porosity beds, such as tidal breccias and microkarst, at sequence boundaries in sequences I–III. These cemented beds and the limestone of sequence IV establish vertical barriers to fluid flow and compartmentalize the Madison Formation into predictable flow units defined by third-order sequence stratigraphy (Westphal et al., 2004). Commonly, hydrothermal activity in carbonates is considered to increase reservoir quality by increasing the porosity and permeability of the host rock; this can be accomplished via fracturing; replacement dolomitization, which increases matrix permeability; and dissolution of the host rock, which results in solution enlargement and increased connectivity of the pore space (Hurley and Budros, 1990; Teare and Reimer, 1992). This is not the case with the Laramide hydrothermal activity because the cementation by late-stage calcite occludes any porosity and permeability created during the tectonic brecciation and fracturing event. The hydrothermal activity ultimately creates unpredictable horizontal heterogeneities to fluid flow by establishing vertically oriented and impermeable corridors in Madison Formation carbonates.

CONCLUSIONS AND IMPLICATIONS

1. Laramide hydrothermal activity occurs throughout the Owl Creek thrust sheet and is responsible for hydrothermal late-stage calcite precipitation. Cementation by late-stage calcite reduces the potential of otherwise high-quality reservoirs in Madison Formation carbonates.
2. Relatively low-saline (<5 wt.% NaCl), radiogenic (0.708948–0.727310), and isotopically depleted ($\delta^{18}O = -26.5$ to -15.1 ‰) hydrothermal fluids migrate vertically along thrust faults connected to deeply buried parts of radiogenic basement rock and fracture and brecciate Madison Formation carbonates during earthquakes. Fracturing and brecciation is episodic and is most intense at the leading edge of the thrust sheet and less so along the basin margins.
3. The $\delta^{13}C$ and $\delta^{18}O$ values, and fluid inclusions suggest that late-stage calcite precipitated from fluids with temperatures between 120 and 180°C. Fluid-inclusion measurements indicate that the calcite precipitated from fluids having minimum entrapment temperatures from 120 to 140°C. Equilibrium between methane and CO_2-bearing fluids at 180°C produces enriched $\delta^{13}C$ values (~10‰), which are within the range of those measured from the leading edge of the Owl Creek thrust sheet (~5–12‰). The $\delta^{18}O$ values indicate that the calcite precipitated from a mixture of downward-percolating meteoric waters and hot subsurface brines.
4. Tectonic-hydrothermal late-stage calcite cementation occludes porosity and reduces permeability created during the brecciation events. This establishes horizontal barriers to fluid flow and compartmentalizes reservoir-quality carbonate. Laramide hydrothermal activity ultimately introduces unpredictable heterogeneities locally and predictable heterogeneities regionally.

5. Petroleum inclusions in late-stage calcite and dolomite rims show that the Madison Formation was charged with hydrocarbons once during pre-Laramide dolomite formation in the burial environment, during the tectonic-hydrothermal activity of the Laramide orogeny, and after.

Orogenic events that affected the Madison Formation may have far-reaching implications for hydrocarbon and groundwater aquifer exploration in other sedimentary basins that developed in compressional regimes. Diagenesis associated with the tectonic-hydrothermal activity can negatively impact lateral permeability pathways and the flow of fluids and gas in otherwise high-quality reservoir rock. Tectonic-hydrothermal diagenesis inherently introduces unpredictable risks at the local field scale, which may significantly affect our ability to recover the original volume estimates of a fluid or gas. Furthermore, the distribution of these features is predictable regionally, and the highest risk is located near and along uplifted basin margins dominated by groundwater chemistry and a hydrological framework characteristic of a compressional orogeny; this tectonic-diagenetic activity is significantly different than the processes operating at the basin center.

REFERENCES CITED

Bellahsen, N., P. Fiore, and, D .D. Pollard, 2004, The role of fractures in the structural interpretation of Sheep Mountain anticline: Geological Society of America Annual Meeting Abstracts with Programs, v. 36, no. 5, p. 267.

Blackstone, D. L. Jr., 1986, Structural geology — North-west margin, Bighorn Basin: Park County, Wyoming, and Carbon County, Montana, *in* P. B. Garrison, ed., Geology of the Beartooth uplift and adjacent basins: Montana Geological Society and Yellowstone–Bighorn Research Association Joint Field Conference and Symposium, p. 125–136.

Blackstone, D. L. Jr., 1988, Traveler's guide to the geology of Wyoming: Geological Survey of Wyoming Bulletin, v. 67, p. 130.

Blackstone, D. L. Jr., and P. W. Huntoon, 1984, Tectonic structures responsible for anisotropic transmissivities in the Paleozoic aquifers of the southern Bighorn Basin: Wyoming: U.S. Geological Survey Research Project Technical Completion Report G-879, no. 2, p. 1–74.

Bliefnick, D. et al., 2000, Diagenetic controls on Visean–Artinskian reservoir heterogeneity in the Karachaganak platform, North Caspian Basin, Kazakhstan, *in* H.-G. Herbig and M. Aretz, eds., Permo-Carboniferous carbonate platforms and reefs: Society of Sedimentary Geology (SEPM) and International Association of Sedimentologists Field Guide, v. 73, p. 11–13.

Bottinga, Y., 1969, Calculated fractionation factors for carbon and hydrogen isotope exchange in the system calcite-CO_2-graphite-methane-hydrogen and water vapor: Geochimica et Cosmochimica Acta, v. 33, p. 49–64.

Bruckschen, P., S. Oesmann, and J. Veizer, 1999, Isotope stratigraphy of the European Carboniferous: Proxy signals for ocean chemistry, climate and tectonics: Chemical Geology, v. 161, 127–163.

Buoniconti, M. R., 2006, The evolution of the carbonate shelf margins and fill of the Antler foreland Basin by prograding Mississippian carbonates, northern U.S. Rockies: Ph.D. dissertation, Rosenstiel School of Marine and Atmospheric Science, University of Miami, Miami, Florida, 430 p.

Burke, R. B., 1994, Mississippian subaerial exposure surfaces within the Sherwood subinterval, Mission Canyon Formation, Lucky Mound field, North Dakota (abs.): AAPG Annual Meeting Program, v. 3, p. 112.

Burke, W. H., R. E. Denison, E. A. Hetherington, R. B. Koepnick, H. F. Nelson, and J. B. Otto, 1982, Variation of seawater $^{87}Sr/^{86}Sr$ throughout Phanerozoic time: Geology, v. 10, p. 516–519.

Choquette, P. W., and N. P. James, 1987, Diagenesis in limestones — 3. The deep burial environment: Geoscience Canada, v. 14, p. 3–35.

Craig, H. L., I. Gordon, and Y. Horibe, 1963, Isotopic exchange effects in the evaporation of water: Journal of Geophysical Research, v. 68, no. 17, p. 5079–5087.

Crockett, J. J., 1994, Porosity evolution of the Madison Limestone (Mississippian): Wind River Basin, Wyoming: M.S. thesis, Lousiana State University, Baton Rouge, Lousiana, 103 p.

Deuser, W. G., 1970, Extreme $^{13}C/^{12}C$ variations in Quaternary dolomites from the continental shelf: Earth and Planetary Science Letters, v. 8, p. 118–124.

Dickinson, W. R., and W. S. Snyder, 1978, Plate tectonics of the Laramide orogeny, *in* V. Matthews, III, ed., Laramide folding associated with basement block faulting in the western United States: Geological Society of America Memoir 151, p. 355–366.

Dickinson, W. R., M. A. Klute, M. J. Hayes, S. U. Janecke, E. R. Lundin, M. A. McKittrick, and M. D. Olivares, 1988, Paleogeographic and paleotectonic setting of Laramide sedimentary basins in the Rocky Mountain region: Geological Society of America Bulletin, v. 100, p. 1023–1039.

Donovan, T. J., 1974, Petroleum micro-seepage at Cement, Oklahoma: Evidence and mechanism: AAPG Bulletin, v. 58, p. 429–446.

Doremus, D. M., 1986, Groundwater circulation and water quality associated with the Madison aquifer in the northeastern Bighorn Basin, Wyoming: M.S. thesis, University of Wyoming, Laramie, Wyoming, 81 p.

Drummond, S. E., and H. Ohmoto, 1985, Chemical evolution and mineral deposition in boiling hydrothermal systems: Economic Geology, v. 80, p. 126–147.

Ducea, M., G. Sen, J. Eiler, and J. Fimbres, 2002, Melt depletion and subsequent metasomatism in the shallow mantle beneath Koolau volcano, Oahu (Hawaii): Geochemistry, Geophysics, Geosystems, v. 3, no. 2, p. 4–17.

Elrick, M., 1990, Development of cyclic ramp-to-basin carbonate deposits, lower Mississippian, Wyoming and Montana: Ph.D. dissertation, Virginia Polytechnic Institute and State University, Virginia, 170 p.

Epstein, S., and T. Mayeda, 1953, Variation of O^{18} content of waters from natural sources: Geochimica et Cosmochimica Acta, v. 4, p. 213–224.

Epstein, S., R. Buchsbaum, H. A. Lowenstam, and H. C. Urey, 1953, Revised carbonate-water isotopic temperature scale: Geological Society of America Bulletin, v. 64, p. 1315–1326.

Erslev, E. A., 1990, Heterogenous Laramide deformation in the Rattlesnake Mountain anticline, Cody, Wyoming, *in* S. Robert, ed., Geologic field tours of western Wyoming and parts of

adjacent Idaho, Montana, and Utah: Wyoming Geological Survey Public Information Circular 29, p. 141–149.

Erslev, E. A., and J. L. Rogers, 1993, Basement-cover geometry of Laramide fault-propagation folds, *in* C. J. Schmidt, R. B. Chase, and E. A. Erslev, eds., Laramide basement deformation in the Rocky Mountain foreland of the western United States: Geological Society of America Special Paper 280, p. 125–146.

Ettenshohn, F. R., 1993, Possible flexural controls on the origins of extensive, ooid-rich, carbonate environments in the Mississippian of the United States, *in* B. D. Keith and C. W. Zuppann, eds., Mississippian oolites and modern analogs: AAPG Studies in Geology 35, p. 13–30.

Faure, G., P. M. Hurley, and H. W. Fairbairn, 1963, An estimate of the isotopic composition of strontium in rocks of the Precambrian shield of North America: Journal of Geophysical Research, v. 68, p. 2323–2329.

Fritz, W. J., and S. Harrison, 1985, Early Tertiary volcaniclastic deposits of the northern Rocky Mountains, *in* R. M. Flores and S. S. Kaplan, eds., Cenozoic paleogeography of the west-central United States: Rocky Mountain Section, SEPM, Rocky Mountain Paleogeography Symposium, v. 3, p. 383–402.

Goldstein, R. H., and T. J. Reynolds, 1994, Systematics of fluid inclusions in diagenetic minerals: SEPM Short Course, v. 31, p. 1–199.

Gries, R. R., 1983, North-south compression of Rocky Mountain foreland structures, *in* J. D. Lowell, ed., Rocky Mountain foreland basins and uplifts: Rocky Mountain Association of Geologists, p. 9–32.

Gutschick, R. C., and C. A. Sandberg, 1983, Mississippian continental margins of the conterminous United States, *in* D. J. Stanley and G. T. Moore, eds., The shelfbreak: Critical interface on continental margins: SEPM Special Publication 33, p. 79–96.

Hanshaw, B. B., J. Busby, and L. Roger, 1978, Geochemical aspects of the Madison aquifer system: Montana Geological Society, 24th Annual Conference, Williston Basin Symposium: Billings, Montana Geological Society, p. 385–390.

Henley, R. W., 1985, The geothermal framework of hydrothermal ore deposits: Reviews in Economic Geology, v. 2, p. 1–44.

Holland, H. D., 1984, The chemical evolution of the atmosphere and oceans: Princeton, New Jersey, Princeton University Press, 582 p.

Hudson, J. D., 1977, Stable isotopes and limestone lithification: Journal of the Geological Society (London), v. 133, p. 637–660.

Humphrey, J. D., E. Poeter, and M. B. Heintz, 2005, Stable oxygen and hydrogen isotopes of precipitation and groundwater in a mountain watershed, Jefferson County, Colorado: Geological Society of America Abstracts with Programs, v. 37, no. 7, p. 361.

Huntoon, P. W., 1993, The influence of Laramide foreland structures on modern ground-water circulation in Wyoming artesian basin, *in* A. W. Snoke, J. R. Steidtmann, and S. M. Roberts, eds., Geology of Wyoming: Geological Survey of Wyoming, Memoir 5, p. 756–789.

Hurley, N. F., and R. Budros, 1990, Albion-Scipio and Stony Point fields–U.S.A. Michigan basin, *in* E. A. Beaumont and N. H. Foster, eds., Stratigraphic traps: I: AAPG Treatise of Petroleum Geology, Atlas of Oil and Gas Fields, p. 1–37.

Irwin, H., C. Curtis, and M. L. Colemen, 1977, Isotopic evidence for source of diagenetic carbonate formed during burial of organic rich sediments: Nature, v. 269, p. 209–213.

James, N. P., and P. W. Choquette, 1983, Diagenesis: 6. Limestones—The seafloor diagenetic environment: Geoscience Canada, v. 10, p. 162–179.

Jarvis, T. W., 1986, Regional hydrogeology of the Paleozoic aquifer system, southeastern Bighorn Basin, Wyoming, with an impact analysis on Hot Springs State Park: M.S. thesis, University of Wyoming, Laramie, Wyoming, 227 p.

Jewell, P. W., N. J. Silberling, and K. M. Nichols, 2000, Geochemistry of the Mississippian Delle phosphatic event, eastern Great Basin, U.S.A.: Journal of Sedimentary Research, v. 70, p. 1222–1233.

Katz, D. A., M. R. Buoniconti, G. P. Eberli, P. K. Swart, and L. B. Smith, Jr., 2005, Positive carbon isotopic excursions and their application to sequence stratigraphy in shallow water carbonates, Mississippian Madison Formation, Wyoming and Montana (abs.): AAPG Annual Meeting Program, v. 14, p. A70–71.

Keefer, W. R., 1965a, Geologic history of the Wind River Basin, Wyoming: AAPG Bulletin, v. 49, p. 1878–1892.

Keefer, W. R., 1965b, Stratigraphy and geologic history of the uppermost Cretaceous, Paleocene, and Eocene rocks in the Wind River Basin, Wyoming: U.S. Geological Survey Professional Paper 495-A, p. 77.

Keefer, W. R., 1970, Structural geology of the Wind River Basin, Wyoming: U.S. Geological Survey Professional Paper 495-D, p. 60.

Keefer, W. R., and J. A. V. Lieu, 1966, Paleozoic formations in the Wind River Basin Wyoming: U.S. Geological Survey Professional Paper 495-B, 60 p.

Kislak, J., L. Smith, D. Peacock, G. Eberli, and P. Swart, 2001, Classification, distribution, and origin of hydrothermal breccias, Madison Formation, Wyoming (abs.): AAPG Annual Meeting Program, v. 10, p. A105.

Kraus, F. F., C. R. Scotese, C. Nieto, S. G. Sayegh, J. C. Hopkins, and R. O. Meyer, 2004, Paleozoic stromatactis and zebra carbonate mud-mounds: Global abundance and paleogeographic distribution: Geology, v. 32, no. 3, p. 181–184.

Lafrenz, W. B., R. D. Shuster, P. A. Mueller, and D. R. Bowes, 1986, Archean and Proterozoic granitoids of the Hawley Mountain area, Beartooth Mountains, Montana: Montana Geological Society, Yellowstone-Bighorn Research Association (YBRA) Field Conference, p. 79–89.

Lloyd, R. M., 1964, Variations in the oxygen and carbon isotope ratios of Florida Bay mollusks and their environmental significance: Journal of Geology, v. 72, p. 84–111.

Lucia, F. J., 1995, Rock-fabric/petrophysical classification of carbonate pore space for reservoir characterization: AAPG Bulletin, v. 79, p. 1275–1300.

Machel, H. G., and J. Lonne, 2002, Hydrothermal dolomite—A product of poor definition and imagination: Sedimentary Geology, v. 152, p. 163–171.

Maughan, E. K., 1983, Tectonic setting of the Rocky Mountain region during the late Paleozoic and early Mesozoic, *in* J. W. Babcock, ed., Proceedings of the Symposium on the Genesis of Rocky Mountain Ore Deposits: Changes with Time and Tectonics: Denver, Regional Exploration Geologists Society, p. 39–50.

McKerrow, W. S., and C. R. Scotese, 1990, Revised world maps and introduction, *in* W. S. McKerrow and C. R. Scotese, eds., Paleozoic paleogeography and biogeography: Geological Society (London) Memoir 12, p. 1–12.

Middleton, G. V., 1961, Evaporite solution breccias from the Mississippian of southwest Montana: Journal of Sedimentary Petrology, v. 31, p. 189–195.

Moore, C. H., 1995, Gas production from a super-deep dolomite reservoir, Madden field, Wind River Basin, Wyoming, U.S.A.: AAPG Hedberg Conference on the Carbonate Reservoirs of the World: Problems, Solutions and Strategies for the Future, Pau, France, session 3, paper 17.

Moore, C. H., 2001, Carbonate reservoirs: Porosity evolution and

diagenesis in a sequence stratigraphic framework: New York, Elsevier, Developments in Sedimentology 55, 444 p.
Morse, J. W., and F. T. Mackenzie, 1990, The CO_2-carbonic acid system and solution chemistry, *in* J. W. Morse and F. T. Mackenzie, Geochemistry of sedimentary carbonates: Developments in Sedimentology 48, p. 1–38.
Murata, K. J., I. Friedman, and B. M. Madsen, 1969, Isotopic composition of diagenetic carbonates in marine Miocene formations of California and Oregon: U.S. Geological Survey Professional Paper 614-B, p. 1–24.
Narr, W., 1993, Deformation of basement in basement-involved, compressive structures, *in* C. J. Schmidt, R. B. Chase, and E. A. Erslev, eds., Laramide basement deformation of the Rocky Mountain foreland of the western United States: Geological Society of America Special Paper 280, p. 107–124.
Nichols, K. M., and N. J. Silberling, 1991, Petrology and depositional setting of Mississippian rocks associated with an anoxic event at Samak, western Uinta Mountains, Utah: Petrology and significance of a Mississippian (Osagean–Meramecian) anoxic event, Lakeside Mountains, northwestern Utah: U.S. Geological Survey Bulletin, v. 1787-ST, p. 25.
Paylor, E. D. II, and H. Lang, 1990, Stratigraphic and structural overview of the Owl Creek Mountains area, Wyoming, *in* S. Robert, ed., Geologic field tours of western Wyoming and parts of adjacent Idaho, Montana, and Utah: Wyoming Geological Survey Public Information Circular 29, p. 151–167.
Paylor, E. D. II, and A. Yin, 1993, Left-slip evolution of the North Owl Creek fault system, Wyoming, during Laramide shortening, *in* C. J. Schmidt, R. B. Chase, and E. A. Erslev, eds., Laramide basement deformation in the Rocky Mountain foreland of the western United States: Geological Society of America Special Paper 280, p. 229–242.
Peterson, J. A., 1986, General stratigraphy and regional paleotectonics of the western Montana overthrust belt, *in* J. A. Peterson, ed., Paleotectonics and sedimentation in the Rocky Mountain region, United States: AAPG Memoir 41, p. 57–86.
Petty, D. M., 1996, Regional stratigraphic and facies relationships in the Mission Canyon Formation, North Dakota portion of the Williston Basin, *in* M. W. Longman and M. D. Sonnenfeld, eds., Paleozoic systems of the Rocky Mountain region: Rocky Mountain Section, SEPM, p. 193–212.
Reid, S. K., 1991, Evolution of the lower Mississippian Mission Canyon platform and Antler foredeep, Montana and Idaho: Ph.D. dissertation, Texas A&M University, College Station, Texas, 105 p.
Robert, F., and W. C. Kelly, 1987, Ore-forming fluids in Archean gold-bearing quartz veins at the Sigma mine, Abitibi greenstone belt, Quebec, Canada: Economic Geology, v. 82, p. 56–74.
Roberts, A. E., 1966, Stratigraphy of the Madison Group near Livingston, Montana, and discussion of karst and solution-breccia features: U.S. Geological Survey Professional Paper P 0526-B, p. B1–B23.
Rose, P. R., 1976, Mississippian carbonate shelf margins, western United States, *in* J. G. Hill, ed., Geology of the Cordilleran hingeline: Rocky Mountain Association of Geologists, p. 135–151.
Sales, J. K., 1983, Collapse of Rocky Mountain basement uplifts, *in* J. D. Lowell, ed., Rocky Mountain foreland basins and uplifts: Rocky Mountain Association of Geologists, p. 79–97.
Saltzman, M. R., E. Groessens, and A. V. Zhuravlev, 2004, Carbon cycle models based on extreme changes in $\delta^{13}C$: An example from the lower Mississippian: Paleogeography, Paleoclimatology, Palaeocology, v. 213, p. 359–377.
Sandberg, C. A., and R. C. Gutschick, 1984, Distribution, microfauna, and source-rock potential of Mississippian Delle phosphatic member of Woodman Formation and equivalents, Utah and adjacent states, *in* J. L. Clayton and F. F. Meissner, eds., Hydrocarbon source rocks of the greater Rocky Mountain region: Rocky Mountain Association of Geologists, p. 135–178.
Sando, W. J., 1967, Madison Limestone (Mississippian) Wind River, Washakie, and Owl Creek Mountains, Wyoming: AAPG Bulletin, v. 51, p. 529–557.
Sando, W. J., 1974, Ancient solution phenomena in the Madison Limestone (Mississippian), east flank of Bighorn Mountains, Wyoming, *in* R. B. Laudon, ed., Geology and energy resources of the Powder River Basin: Wyoming Geological Association 28th Annual Field Conference Guidebook, p. 45–51.
Sando, W. J., 1976, Mississippian history of the northern Rocky Mountains region: U.S. Geological Survey Journal of Research, v. 4, p. 317–338.
Sando, W. J., 1988, Madison Limestone (Mississippian) paleokarst: A geologic synthesis, *in* N. P. James and P. W. Choquette, eds., Paleokarst: New York, Springer-Verlag, p. 256–277.
Sando, W. J., M. Gordon, Jr., and J. T. Dutro, Jr., 1975, Stratigraphy and geologic history of the Amsden Formation (Mississippian and Pennsylvanian) of Wyoming: U.S. Geological Survey Professional Paper 858-A, p. 78.
Sando, W. J., C. A. Sandberg, and W. J. Perry, Jr., 1985, Revision of Mississippian stratigraphy, northern Montana, southwest Montana: U.S. Geological Survey Bulletin, v. 1656-A, p. 10.
Savage, H. M., and M. L. Cooke, 2004, The effect of non-parallel thrust fault interaction on fold patterns: Journal of Structural Geology, v. 26, p. 905–917.
Scholle, P. A., and D. S. Ulmer-Scholle, 2003, 23-Syngenetic/eogenetic marine diagenesis, *in* P. A. Scholle and D. S. Ulmer-Scholle, eds., A color guide to the petrography of carbonate rocks: Grains, textures, porosity, diagenesis: AAPG Memoir 77, p. 313–327.
Sibson, R. H., 1985, Stopping of earthquake ruptures at dilational fault jogs: Nature, v. 316, p. 248–251.
Sibson, R. H., 1990, Faulting and fluid flow, *in* B. E. Nesbitt, ed., Short course on fluids in tectonically active regimes of the continental crust: Mineralogical Association of Canada Short Course Handbook, v. 18, p. 93–131.
Silberling, N. J., K. M. Nichols, J. H. Trexler, Jr., P. W. Jewell, and R. A. Crosbie, 1997, Overview of Mississippian depositional and paleotectonic history of the Antler foreland, eastern Nevada and western Utah, *in* P. K. Link, and B. J. Kowallis, eds., Proterozoic to recent stratigraphy, tectonics, and volcanology, Utah, Nevada, southern Idaho and central Mexico: Brigham Young University, Geology Studies, v. 42, part 1, p. 161–196.
Smith, T. M., 1991, Diagenesis of shallow marine carbonate rocks: Isotopic and trace element constraints from the Mississippian Mission Canyon Formation, central and southwestern Montana: Ph.D. dissertation, Texas A&M University, College Station, 126 p.
Smith, T. M., and S. L. Dorobek, 1993, Alteration of early formed dolomite during shallow to deep burial: Mississippian Mission Canyon Formation, central to southwestern Montana: Geological Society of America Bulletin, v. 105, p. 1389–1399.
Smith, L. B. Jr., G. P. Eberli, and M. D. Sonnenfeld, 2004, Sequence-stratigraphic and paleogeographic distribution of reservoir-quality dolomite, Madison Formation, Wyoming and Montana, *in* G. M. Grammer, G. P. Eberli, and P. M. Harris, eds., Integration of outcrop and modern analogues in reservoir modeling: AAPG Memoir 80, p. 94–118.
Sonnenfeld, M. D., 1996a, Sequence evolution and hierarchy within the lower Mississippian Madison Limestone of Wyoming, *in* M. W. Longman and M. D. Sonnenfeld, eds., Paleozoic systems of the Rocky Mountain region: Rocky Mountain Section, SEPM, p. 165–192.
Sonnenfeld, M. D., 1996b, An integrated sequence stratigraphic

approach to reservoir characterization of the lower Mississippian Madison Limestone, emphasizing Elk Basin field, Bighorn Basin, Wyoming: Ph.D. dissertation, Colorado School of Mines, Golden, Colorado, 437 p.

Spencer, S. A., 1986, Groundwater movement in the Paleozoic rocks and impact of petroleum production on water levels in the southwestern Bighorn Basin, Wyoming: M.S. thesis, University of Wyoming, Laramie, Wyoming, 165 p.

Stearns, D. W., 1970, Drape folds over uplifted basement blocks with emphasis on the Wyoming province: Ph.D. dissertation, Texas A&M University, College Station, 118 p.

Stone, D. S., 1993, Basement-involved thrust-generated folds as seismically imaged in the subsurface of the central Rocky Mountain foreland, *in* C. J. Schmidt, R. B. Chase, and E. A. Erslev, eds., Laramide basement deformation in the Rocky Mountain foreland of the western United States: Geological Society of America Special Paper 280, p. 271–318.

Teare, M. R., and J. D. Reimer, 1992, Thermochemical sulfate reduction and hydrothermal dolomitization (TSR-HTD); a diagenetic process that created and modified Middle Devonian reservoirs in northeastern British Columbia: AAPG and SEPM Annual Meeting Program, p. 130.

Tucker, M. E., and V. P. Wright, 1990, Radiogenic isotopes, *in* M. E. Tucker, P. V. Wright, and J. A. D. Dickson, eds., Carbonate sedimentology: Oxford, United Kingdom, Blackwell Science Publishing (GBR), p. 312.

Veizer, J., D. Ala, K. Azmy, P. Bruckschen, D. Buhl, F. Bruhn, 1999, $^{87}Sr/^{86}Sr$, $\delta^{13}C$, $\delta^{18}O$ evolution of Phanerozoic seawater: Chemical Geology, v. 161, p. 59–88.

Westphal, H., G. P. Eberli, L. B. Smith, G. M. Grammer, and J. Kislak, 2004, Reservoir characterization of the Mississippian Madison Formation, Wind River Basin, Wyoming: AAPG Bulletin, v. 88, no. 4, p. 405–432.

White, D. E., 1957, Thermal waters of volcanic origin: Geological Society of America Bulletin, v. 68, p. 1637–1658.

Witkind, I. J., and L. T. Grose, 1972, Geologic atlas of the Rocky Mountain region: Rocky Mountain Association of Geologists, 34 p.